




Heparanase Blockade as a Novel Dual-Targeting Therapy for COVID-19

Jingyu Xiang,^a Mijia Lu,^b Min Shi,^{c,d} Xiaogang Cheng,^a Kristin A. Kwakwa,^a Jennifer L. Davis,^a Xinming Su,^a Suzanne J. Bakewell,^a Yuexiu Zhang,^b Francesca Fontana,^a Yalin Xu,^a Deborah J. Veis,^e John F. DiPersio,^a Lee Ratner,^a Ralph D. Sanderson,^f Alessandro Nosedà,^g Shamim Mollah,^{c,d}  Jianrong Li,^b Katherine N. Weilbaecher^a

^aDepartment of Medicine, Division of Oncology, Washington University School of Medicine, St. Louis, Missouri, USA

^bDepartment of Veterinary Biosciences, College of Veterinary Medicine, The Ohio State University, Columbus, Ohio, USA

^cDepartment of Genetics, Washington University School of Medicine, St. Louis, Missouri, USA

^dInstitute for Informatics, Washington University School of Medicine, St. Louis, Missouri, USA

^eDepartment of Medicine, Division of Bone and Mineral Diseases, Washington University School of Medicine, St. Louis, Missouri, USA

^fDepartment of Pathology, University of Alabama at Birmingham, Birmingham, Alabama, USA

^gLeadiant Biosciences S.p.A., Rome, Italy

ABSTRACT The coronavirus disease 2019 (COVID-19) pandemic, caused by severe acute respiratory syndrome coronavirus 2 (SARS-CoV-2), has caused over 5 million deaths worldwide. Pneumonia and systemic inflammation contribute to its high mortality. Many viruses use heparan sulfate proteoglycans as coreceptors for viral entry, and heparanase (HPSE) is a known regulator of both viral entry and inflammatory cytokines. We evaluated the heparanase inhibitor Roneparstat, a modified heparin with minimum anticoagulant activity, in pathophysiology and therapy for COVID-19. We found that Roneparstat significantly decreased the infectivity of SARS-CoV-2, SARS-CoV-1, and retroviruses (human T-lymphotropic virus 1 [HTLV-1] and HIV-1) *in vitro*. Single-cell RNA sequencing (scRNA-seq) analysis of cells from the bronchoalveolar lavage fluid of COVID-19 patients revealed a marked increase in *HPSE* gene expression in CD68⁺ macrophages compared to healthy controls. Elevated levels of *HPSE* expression in macrophages correlated with the severity of COVID-19 and the expression of inflammatory cytokine genes, including *IL6*, *TNF*, *IL1B*, and *CCL2*. In line with this finding, we found a marked induction of *HPSE* and numerous inflammatory cytokines in human macrophages challenged with SARS-CoV-2 S1 protein. Treatment with Roneparstat significantly attenuated SARS-CoV-2 S1 protein-mediated inflammatory cytokine release from human macrophages, through disruption of NF- κ B signaling. *HPSE* knockdown in a macrophage cell line also showed diminished inflammatory cytokine production during S1 protein challenge. Taken together, this study provides a proof of concept that heparanase is a target for SARS-CoV-2-mediated pathogenesis and that Roneparstat may serve as a dual-targeted therapy to reduce viral infection and inflammation in COVID-19.

IMPORTANCE The complex pathogenesis of COVID-19 consists of two major pathological phases: an initial infection phase elicited by SARS-CoV-2 entry and replication and an inflammation phase that could lead to tissue damage, which can evolve into acute respiratory failure or even death. While the development and deployment of vaccines are ongoing, effective therapy for COVID-19 is still urgently needed. In this study, we explored HPSE blockade with Roneparstat, a phase I clinically tested HPSE inhibitor, in the context of COVID-19 pathogenesis. Treatment with Roneparstat showed wide-spectrum anti-infection activities against SARS-CoV-2, HTLV-1, and HIV-1 *in vitro*. In addition, HPSE blockade with Roneparstat significantly attenuated SARS-CoV-2 S1 protein-induced inflammatory cytokine release from human macrophages through disruption of NF- κ B signaling. Together, this study provides a proof of principle for the use of Roneparstat as a dual-targeting therapy for COVID-19 to decrease

Editor Bryan R. G. Williams, Hudson Institute of Medical Research

Copyright © 2022 American Society for Microbiology. All Rights Reserved.

Address correspondence to Katherine N. Weilbaecher, kweilbae@wustl.edu.

The authors declare a conflict of interest. Roneparstat (SST0001) is a proprietary drug of Leadiant Biosciences S.p.A. Alessandro Nosedà is the employee of Leadiant Biosciences S.p.A. No potential conflicts of interest were disclosed by the other authors.

Received 13 January 2022

Accepted 27 February 2022

Published 23 March 2022

viral infection and dampen the proinflammatory immune response mediated by macrophages.

KEYWORDS heparanase, COVID-19, macrophage, inflammatory cytokine release, SARS-CoV-2

Coronavirus disease 2019 (COVID-19), caused by severe acute respiratory syndrome coronavirus 2 (SARS-CoV-2), has quickly become a leading cause of death worldwide. In response to the rapid spread of COVID-19, a global effort has been poured into the development of novel therapies for the prevention and treatment of the disease (1). Currently, therapeutic approaches for hospitalized patients with COVID-19 disease include remdesivir, steroids, heparin, convalescent-phase plasma, and monoclonal antibodies, which have had some success, yet the mortality rate remains high in patients with severe disease (2). In contrast to the great success in vaccine development, the progress for effective COVID-19 treatment has been slower.

The complex pathogenesis of COVID-19 consists of two major pathological phases: (i) an early infection phase, characterized by SARS-CoV-2 viral entry, replication, and spread, and (ii) an inflammation phase, characterized by aberrant proinflammatory cytokine release that leads to tissue damage, which can evolve into acute respiratory distress syndrome (ARDS) and hypoxemia that may require mechanical ventilation (3). About 20% of COVID-19 patients progress to the severe/critical stage, featuring a marked increase in inflammatory markers, including C-reactive protein, ferritin, and interleukin-6 (IL-6) (4). In these patients, a “cytokine storm” or “cytokine release syndrome” (CRS) results from excessive noneffective host immune responses by T cells and inflammatory monocytes, a phenomenon often seen in patients receiving chimeric antigen receptor (CAR) T-cell therapy, and is associated with mortality (5).

Similar to SARS-CoV-1 and Middle East respiratory syndrome coronavirus (MERS-CoV), the spike (S) glycoprotein is required for the entry of SARS-CoV-2 into host cells (6). Because of the potent immune response that it elicits, the S protein has also been widely used as the target antigen in COVID-19 vaccines (7). S protein-mediated SARS-CoV-2 entry is codependent on host angiotensin-converting enzyme 2 (ACE2) and heparan sulfate (HS); treatment with heparin or heparin derivatives can decrease SARS-CoV-2 entry (8). Heparan sulfate proteoglycans (HSPGs) on the surface of cells are ubiquitously presented glycoproteins comprised of linear, negatively charged polysaccharide chains that bind to a variety of soluble and insoluble cell surface or extracellular matrix proteins. Many viruses, including herpes simplex virus 1 (HSV-1), dengue virus (DENV), human papillomavirus (HPV), and human T-lymphotropic virus 1 (HTLV-1), exploit cell surface HSPGs by utilizing them to attach to host cells (9).

The enzyme heparanase (HPSE) is the only known mammalian endoglycosidase capable of degrading the heparan sulfate chains of HSPGs and regulating the expression of multiple inflammatory cytokine genes (10, 11). Heparanase has been implicated in the pathogenesis of multiple cancers and inflammatory diseases such as pancreatitis, colitis, and acute renal injury (12, 13). In a model of murine experimental sepsis that results in a systemic inflammatory response and acute lung injury, vascular hyperpermeability and ARDS were eliminated by blocking heparanase degradation of the endothelial glycocalyx (14). In HSV-1-mediated inflammatory disease, heparanase promotes viral shedding and release and triggers proinflammatory cytokine release (15). A recent clinical study reported an increase in plasma heparanase levels in COVID-19 patients, especially in patients with severe disease (16). However, the contribution of heparanase to the pathogenesis of COVID-19 has not been fully characterized.

Due to the elevated expression of heparanase in cancers such as multiple myeloma (MM), several heparanase inhibitors have been developed as anticancer therapies (10). Roneparstat (SST0001) is a chemically modified, 100% N-acetylated, and glycol-split heparin and a potent inhibitor of heparanase enzyme activity (IC_{50} [half-maximal inhibitory concentration] = 3 nM) (17). Glycol splitting of uronic acid residues within heparin disrupts an essential glucuronic acid that lies within the heparin pentasaccharide

responsible for binding to antithrombin (18). The resulting diminished antithrombin binding activity of the glycol-split heparin greatly diminishes its anticoagulant activity, thus allowing the utilization of the drug at high doses in patients. At the preclinical stage, Ronaparstat also showed therapeutic benefit in multiple inflammatory disease models such as acute pancreatitis and acute kidney injury (19). In a phase I clinical trial (ClinicalTrials.gov identifier NCT01764880) in patients with advanced MM, Ronaparstat was well tolerated and safe at all doses tested, with no dose-limiting toxicities (20).

In this study, we set out to investigate the role of heparanase in the pathogenesis of COVID-19 and evaluate Ronaparstat as a novel therapy. In line with the role of HSPGs as coreceptors for viral entry, we found that treatment with heparin or Ronaparstat effectively decreased the infectivities of SARS-CoV-2 as well as the retroviruses HTLV-1 and HIV-1 *in vitro*. Using HIV-1 Δ env pseudotyped with vesicular stomatitis virus G (VSVg) envelope, an HSPG-independent pseudotyped virus, we further showed that the antiviral activity of Ronaparstat is specific to HSPG-mediated viral entry. Single-cell RNA sequencing (scRNA-seq) analysis of cells isolated from bronchoalveolar lavage fluid (BALF) of COVID-19 patients showed elevated levels of *HPSE* gene expression compared to healthy controls. In addition, we found that *HPSE* expression was almost exclusively upregulated in CD68⁺ macrophages and correlated with disease severity and multiple inflammatory cytokine genes, including *IL6*, *IL1B*, and *TNF*. In primary human macrophages, SARS-CoV-2 S protein challenge induced the expression of *HPSE* and inflammatory cytokines. The knockdown (KD) of *HPSE* in human macrophages attenuated the induction of multiple inflammatory cytokines by SARS-CoV-2 S1 protein, suggesting that *HPSE* plays an important role in the induction of these inflammatory cytokines in macrophages. We further demonstrated that heparanase blockade with Ronaparstat attenuated the production of the inflammatory cytokines in a dose-dependent manner via disruption of NF- κ B signaling. Overall, this study provides a proof of principle for the use of Ronaparstat as a dual-targeting therapy for COVID-19 to decrease viral infection and dampen the proinflammatory immune response mediated by macrophages.

RESULTS

The heparanase inhibitor Ronaparstat decreases SARS-CoV-2 infectivity. Heparan sulfate (HS) is an important cofactor for the attachment and entry of multiple viruses, including SARS-CoV-2 (8, 9). To test whether Ronaparstat could suppress SARS-CoV-2 S protein-mediated entry, we first used a replication-competent VSV-SARS-CoV-2 chimeric virus (VSV-eGFP-SARS-CoV-2), in which the VSV G gene was replaced by the SARS-CoV-2 S gene (Fig. 1A). In this model, Vero-E6 cells were infected by VSV-eGFP-SARS-CoV-2 (multiplicity of infection [MOI] = 0.1) in the presence of various doses of Ronaparstat or heparin for 1 h. At 10 h postinfection, green fluorescent protein-positive (GFP⁺) cells were quantified. Treatment with Ronaparstat or heparin resulted in a significant dose-dependent decrease in infected cells (Fig. 1B and C), with half-maximal inhibitory concentrations (IC₅₀s) of 0.05 μ g/mL and 0.03 μ g/mL, respectively (Fig. 1D and E). Similar inhibitory effects on infectivity were observed in Vero-E6 cells infected with the VSV-eGFP-SARS-CoV-1 chimeric virus in which VSV G was replaced with the SARS-CoV-1 S gene (Fig. 1F to J), suggesting that Ronaparstat and heparin inhibit cell entry mediated by S protein.

We next examined the effect of Ronaparstat and heparin during SARS-CoV-2 infection in Vero-E6 cells. Vero-E6 cells were infected with SARS-CoV-2 in the presence of various doses of Ronaparstat or heparin for 1 h. At 24 h postinfection, the cell culture supernatant from each well was harvested for virus titration by a plaque assay on Vero-E6 cells. SARS-CoV-2-infected Vero-E6 cells were immunostained with specific anti-spike (S) or -nuclear (N) protein antibody (Fig. 1K and L). In line with what we observed in the VSV-eGFP-SARS-CoV-2 infection assay, both Ronaparstat and heparin treatment significantly decreased SARS-CoV-2 infection, with IC₅₀s of 0.07 μ g/mL and 0.05 μ g/mL, respectively (Fig. 1M and N). Together, these data demonstrated that Ronaparstat is potent against SARS-CoV-2 infection *in vitro*.

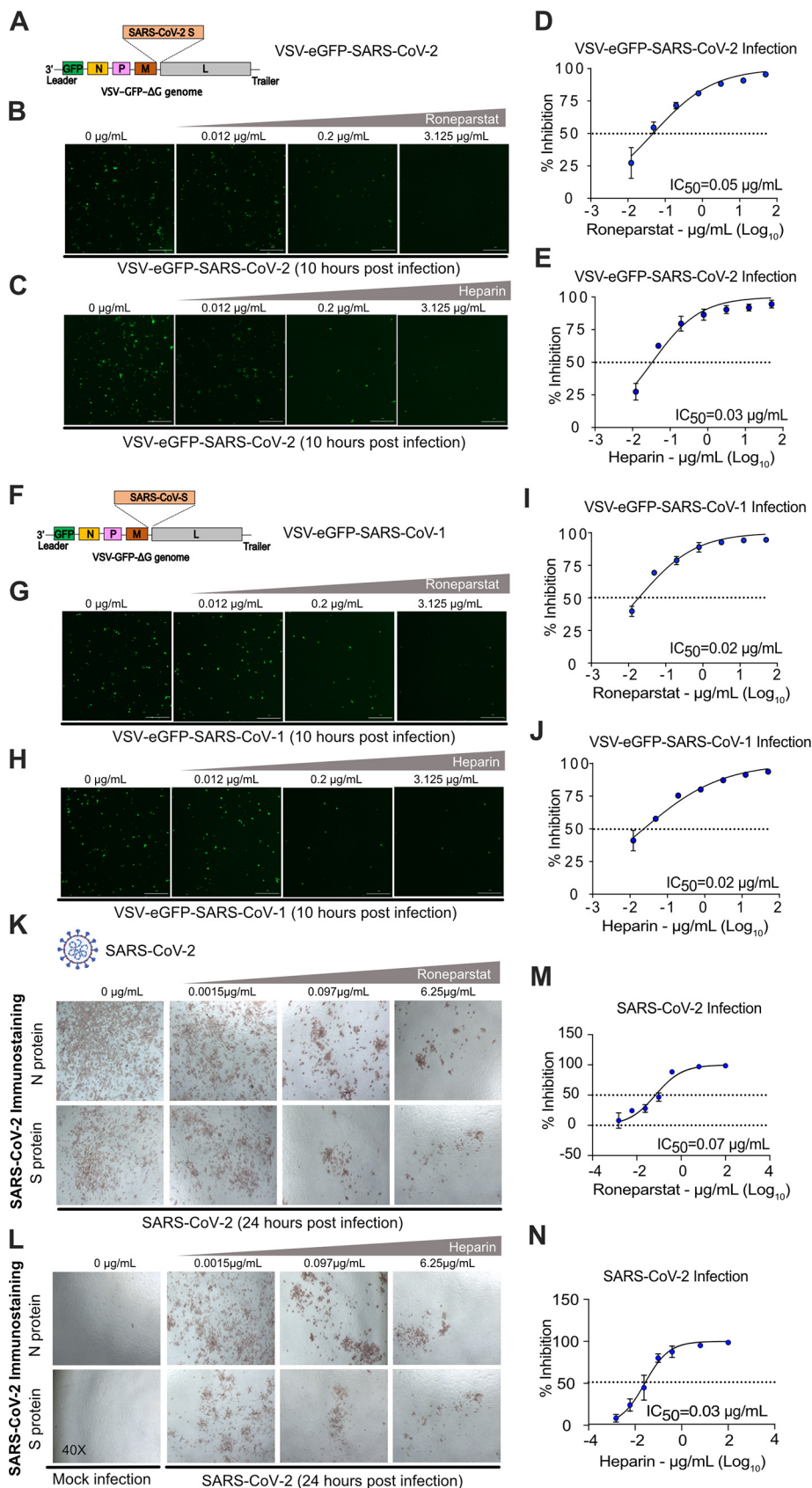


FIG 1 The HPSE inhibitor Roneparstat suppresses coronavirus infection. (A) Schematic representation of the genome of VSV-eGFP-SARS-CoV-2. VSV G was deleted from the VSV genome, and the SARS-CoV-2 S (Continued on next page)

Roneparstat blocks HSPG-dependent viral entry. To rule out that the reduction of infectivity was due to the potential cytotoxicity of Roneparstat, we examined the viability of cells treated with various doses (up to 200 $\mu\text{g}/\text{mL}$) of Roneparstat. As measured by cell viability assays, no cytotoxicity was observed in multiple cell lines (Vero-E6, Jurkat, and THP-1) treated with Roneparstat (Fig. 2A to C). HSPG is known as one of the coreceptors for SARS-CoV-2 and HTLV-1 viral entry (8). Therefore, we further extended our analysis to the infectivity of retroviruses, including HTLV-1 and HIV-1. Jurkat T cells, engineered to express the luciferase (Luc) gene driven by the HTLV-1 long terminal repeat (LTR), were cocultured with the HTLV-1-producing cell line MT-2 for 48 h in the presence or absence of various doses of Roneparstat. Similarly, TZM-Blue cells engineered to express luciferase driven by the HIV-1 LTR were pretreated with various doses of Roneparstat and infected with HIV-1 for 24 h. In both experiments, Roneparstat treatment significantly decreased infection by HTLV-1 (Fig. 2D) and HIV-1 (both CXCR4- and CCR5-tropic strains) (Fig. 2E and F). Conversely, infection by VSV is independent of the HSPG-mediated viral entry mechanism (21, 22). To confirm that the reduction of infectivity by Roneparstat was HSPG dependent, we constructed HSPG-independent VSVg-HIV-1 Δenv pseudotyped virus by cotransfecting HIV-1-luc/ Δenv (HIV-1 with defective envelope) with VSVg. CXCR4-expressing U87/X4 or CCR5-expressing U87/R5 target cells were infected with VSVg-HIV-1 Δenv -luc in the presence or absence of Roneparstat for 48 h. No reduction of infectivity was observed in either U87/X4 or U87/R5 cells infected with VSVg-HIV-1 Δenv -luc (Fig. 2G and H), suggesting that Roneparstat-mediated blockade of infectivity is through HSPGs. Together, these data demonstrated that treatment with Roneparstat or heparin decreases the infectivity of a broad spectrum of viruses, including SARS-CoV-1, SARS-CoV-2, HTLV-1, and HIV-1, *in vitro* through an HSPG-dependent viral entry mechanism.

Upregulation of heparanase expression in pulmonary macrophages from COVID-19 patients. Increased plasma levels of heparanase were reported in COVID-19 patients (16). Seeking to identify the cells that expressed the *HPSE* gene in COVID-19 patients, we analyzed the single-cell RNA sequencing (scRNA-seq) data set (GEO accession number [GSE145926](#)) from cells harvested from the bronchoalveolar lavage fluid (BALF) of moderate or severe COVID-19 patients and healthy volunteers (23). *HPSE* gene expression was upregulated in various BALF cell populations of patients with COVID-19, especially those with severe COVID-19 (Fig. 3A). Specifically, *HPSE* was highly expressed in the macrophage population (CD68⁺), with modest increases in T cells (CD3D⁺), epithelial cells (TPPP3⁺ KRT18⁺), and myeloid dendritic cells (mDCs) (CD1C⁺ CLEC9A⁺) in patients with severe COVID-19 compared to the healthy controls and those with moderate disease (Fig. 3B). Further analysis of the CD68⁺ macrophage population demonstrated that

FIG 1 Legend (Continued)

gene was inserted between the M and L genes in the VSV genome, which resulted in the construction of replication-competent VSV-eGFP-SARS-CoV-2. Monolayers of Vero-E6 cells were infected with VSV-eGFP-SARS-CoV-2 at an MOI of 0.1 in the presence or absence of various doses of Roneparstat or heparin for 1 h. At 10 h postinfection, infected cells (GFP⁺) were quantified by a Cytation 5 microscope. (B and C) Representative fluorescence images of Vero-E6 cells infected with VSV-eGFP-SARS-CoV-2 in the presence of 0, 0.012, 0.2, and 3.125 $\mu\text{g}/\text{mL}$ of Roneparstat or heparin. (D and E) Logistic inhibition curve of Roneparstat or heparin treatment during VSV-eGFP-SARS-CoV-2 infection. (F) Schematic representation of the genome of VSV-eGFP-SARS-CoV-1. VSV G was deleted from the VSV genome, and the SARS-CoV-1 S gene was inserted between the M and L genes in the VSV genome, which resulted in the construction of replication-competent VSV-eGFP-SARS-CoV-1. Monolayers of Vero-E6 cells were infected with VSV-eGFP-SARS-CoV-1 at an MOI of 0.1 in the presence or absence of various doses of Roneparstat or heparin for 1 h. At 10 h postinfection, infected cells (GFP⁺) were quantified by a Cytation 5 microscope. (G and H) Representative fluorescence images of Vero-E6 cells infected with VSV-eGFP-SARS-CoV-1 in the presence of 0, 0.012, 0.2, and 3.125 $\mu\text{g}/\text{mL}$ of Roneparstat or heparin. (I and J) Logistic inhibition curve of Roneparstat or heparin treatment during VSV-eGFP-SARS-CoV-1 infection. (K and L) Representative images of immunostaining from SARS-CoV-2 (strain USA-WA1/2020) (400 PFU)-infected monolayers of Vero-E6 cells. Antibodies specific to the SARS-CoV-2 spike (S) or nuclear (N) protein were used to identify SARS-CoV-2-infected cells under various Roneparstat or heparin treatment conditions (0, 0.0015, 0.097, and 6.25 $\mu\text{g}/\text{mL}$). (M and N) Logistic inhibition curve of Roneparstat or heparin treatment during SARS-CoV-2 infection. Error bars represent the SEM. *, $P < 0.05$; **, $P < 0.01$; ***, $P < 0.001$ (2-tailed distribution, homoscedastic Student's *t* test for 2 groups or 1-way ANOVA for multiple comparisons).

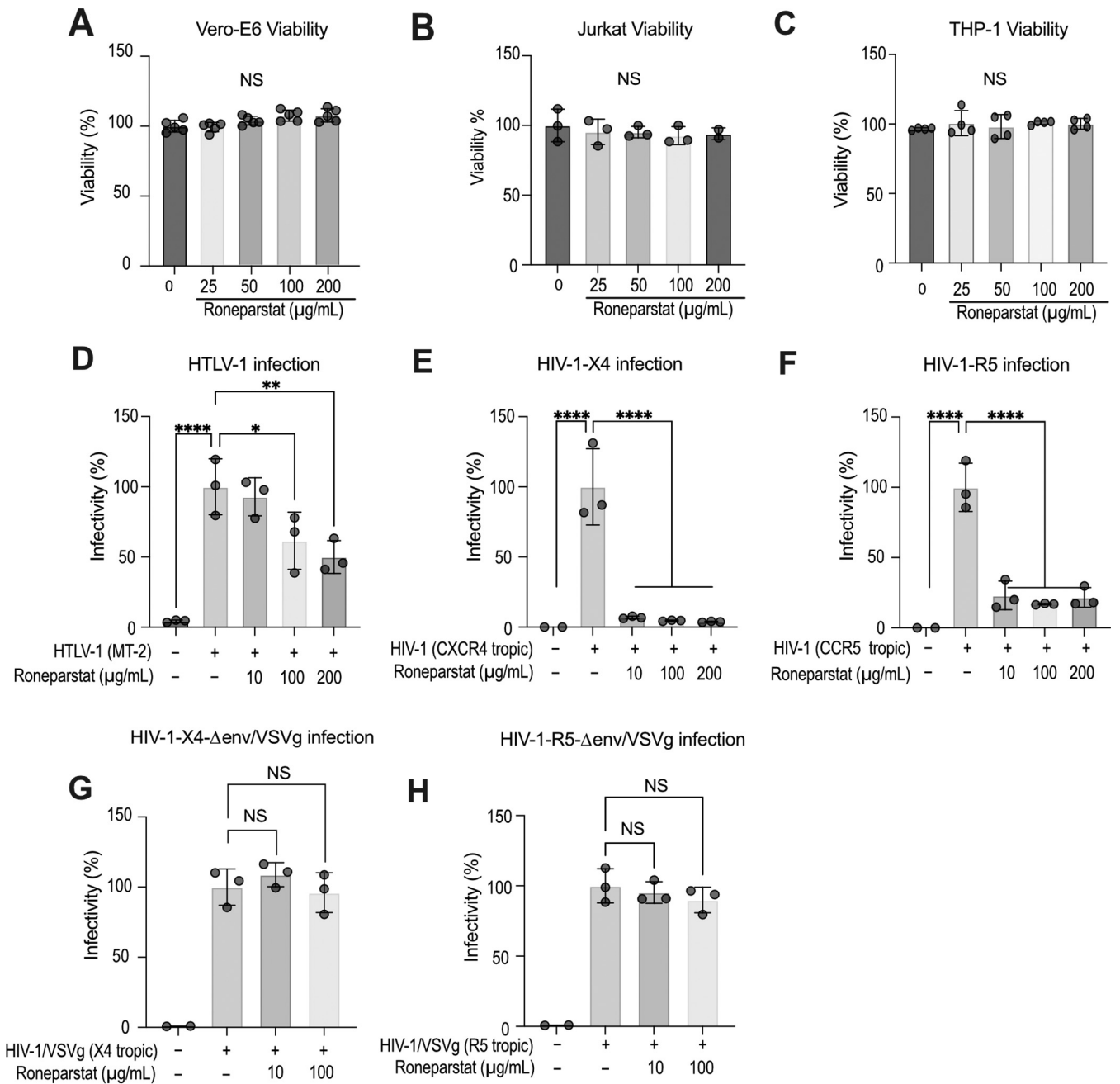


FIG 2 Roneparstat-mediated blockade of infection is dependent on HSPGs. (A to C) The Vero-E6 (A), Jurkat (B), or THP-1 (C) cell line was treated with various doses of Roneparstat (0, 25, 50, 100, and 200 μg/mL) for 24 h. Subsequently, cell viability was examined using a CellTiter-Blue viability assay. (D) Jurkat-LTR-Luc reporter cells cocultured with irradiated HTLV-1-producing MT-2 cells in the presence or absence of various doses (10, 100, and 200 μg/mL) of Roneparstat for 48 h. Infectivity (percent) was quantified via luciferase assays. (E and F) HIV-1-LTR-Luc reporter cells were pretreated overnight with Roneparstat (10, 100, and 200 μg/mL), followed by HIV-1 (CXCR4- or CCR5-tropic strain) infection for 24 h. Infectivity (percent) was quantified via luciferase assays. (G and H) U87/X4 or U87/R5 target cells were infected with the VSVg-pseudotyped virus VSVg-HIV-1Δenv-luc for 48 h in the presence or absence of Roneparstat (10 and 100 μg/mL). Infectivity (percent) was quantified via luciferase assays. Error bars represent the SEM. *, $P < 0.05$; **, $P < 0.01$; ***, $P < 0.001$; NS, not significant (2-tailed distribution, homoscedastic Student's t test for 2 groups or 1-way ANOVA for multiple comparisons).

the expression levels of *HPSE*, along with inflammatory cytokine genes such as *IL6*, *TNF*, *IL1B*, and *CCL2*, increased with the disease severity of COVID-19 (Fig. 3C to G). Inflammatory cytokines such as IL-6 and tumor necrosis factor alpha (TNF-α) are critical players during the inflammation phase of COVID-19 (24). Spearman's correlation coefficient test between *HPSE* and the inflammatory cytokine genes *IL6*, *TNF*, *IL1B*, and *CCL2* showed a significant positive correlation (Fig. 3H to K). These data confirmed that *HPSE* is upregulated in the macrophages of COVID-19 patients and is associated with inflammatory cytokine release.

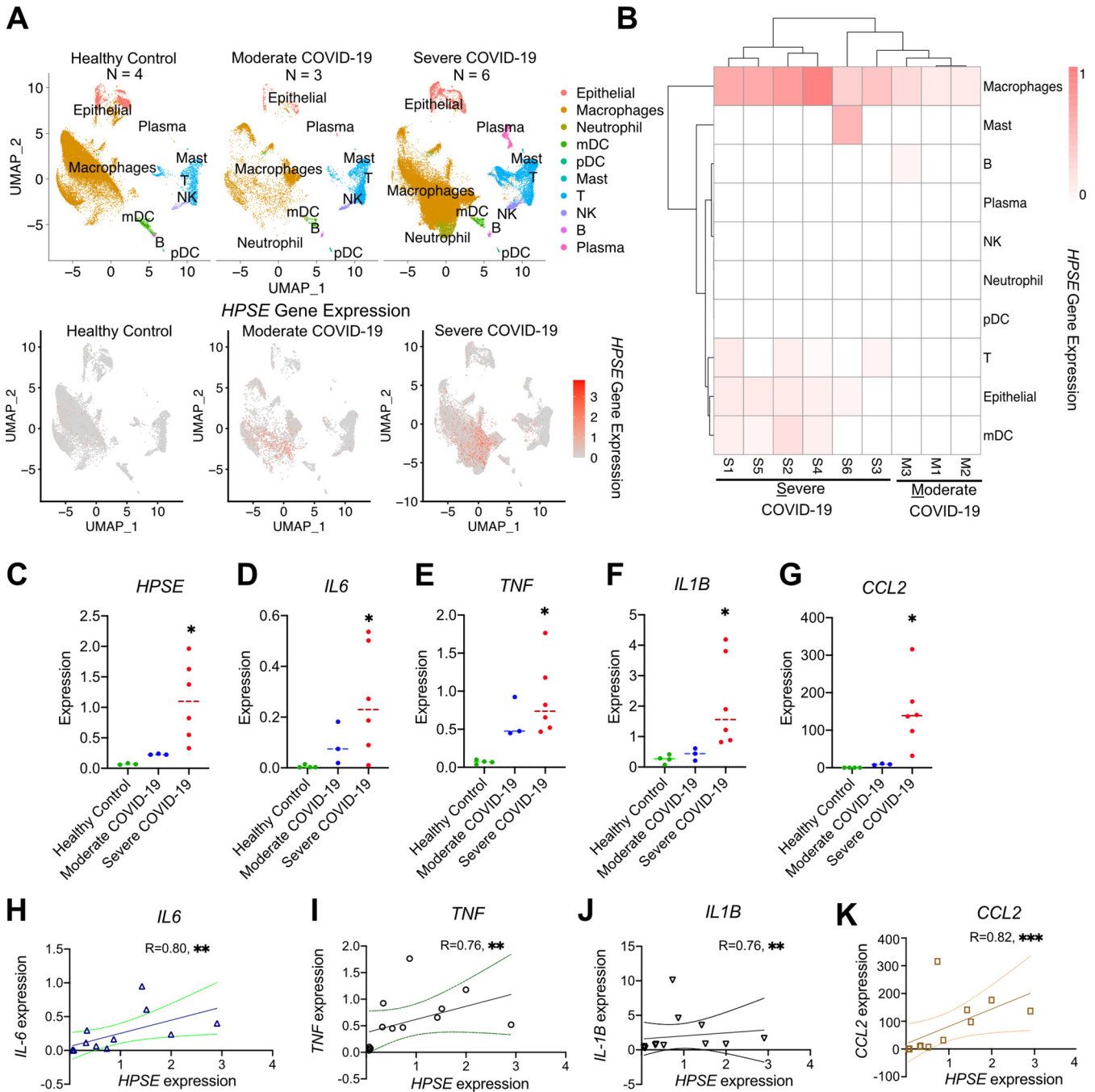


FIG 3 The *HPSE* gene is upregulated in the BALF of COVID-19 patients and correlates with the expression of inflammatory cytokine genes in macrophages. (A, top) Alignment of major BALF cell clusters by UMAP across control ($n = 4$), moderate COVID-19 ($n = 3$), and severe COVID-19 ($n = 6$) samples. (Bottom) UMAP presentation showing the *HPSE* gene expression levels across control, moderate COVID-19, and severe COVID-19 samples. (B) Heat map of differential *HPSE* gene expression of different cell types by each COVID-19 sample. Cell markers (cell types are identified by signature genes) for each cell type are defined as follows: CD68 for macrophages, TPSB2 for mast cells, MS4A1 for B cells, IGHG4 for plasma cells, KLRD1 for natural killer (NK) cells, FCGR3B for neutrophils, LILRA4 for plasmacytoid dendritic cells (pDC), CD3D for T cells, TPPP3 and KRT18 for epithelial cells, and CD1C and CLEC9A for myeloid dendritic cells (mDC). (C to G) Expression levels of *HPSE*, *IL6*, *TNF*, *IL1B*, and *CCL2* by BALF macrophages across healthy control, moderate COVID-19, and severe COVID-19 samples. (H to K) Correlations between *HPSE* expression and the expression of *IL6*, *TNF*, *IL1B*, and *CCL2*. Error bars represent the SEM. *, $P < 0.05$; **, $P < 0.01$; ***, $P < 0.001$ (2-tailed distribution, homoscedastic Student's t test for 2 groups or 1-way ANOVA for multiple comparisons; a Spearman correlation coefficient test was adopted to determine statistically significant correlations between two groups).

Inhibition of HPSE enzyme activity with Roneparstat decreases inflammatory cytokine release induced by SARS-CoV-2 spike protein in human primary macrophages.

The binding of SARS-CoV-2 to host cell coreceptors is mediated by the receptor binding domain (RBD) in the S1 subunit of the spike protein. To test whether S1 protein is

sufficient to trigger inflammatory cytokine release and *HPSE* expression, we used a macrophage challenge model. Human primary macrophages were differentiated from monocytes from healthy human donors *in vitro* and subsequently challenged with SARS-CoV-2 S1 protein overnight (Fig. 4A). Gene expression analysis by quantitative PCR (qPCR) revealed a significant upregulation of *HPSE*, *IL6*, *TNF*, *CCL2*, and *IFNG* after S1 protein challenge (Fig. 4B). To evaluate whether heparanase can regulate the expression of inflammatory cytokine genes such as IL-6, in parallel with S1 protein challenge, we treated macrophages with various doses of active recombinant human heparanase for 12 h and examined the IL-6 expression level by qPCR. Treatment with exogenous heparanase induced elevated levels of IL-6 expression, at levels similar to those seen with S1 protein stimulation (Fig. 4C). Next, to examine whether HPSE blockade could suppress the induction of inflammatory cytokines, we challenged macrophages with S1 protein, in the presence or absence of various doses of Ronaparstat. Indeed, treatment with Ronaparstat resulted in a dose-dependent reduction in the expression of inflammatory cytokine genes such as *IL6*, *TNF*, *CCL2*, and *IFNG* (Fig. 4D to G). Using a flow cytometry-based multiplex inflammatory cytokine array, we showed that HPSE blockade with Ronaparstat also significantly attenuated the protein levels of multiple inflammatory cytokines, including IL-6, TNF- α , IL-10, IL-1 β , IL-23, IL-33, and IL-12p70 (Fig. 4H to N). In contrast, no significant changes were seen in interferon gamma (IFN- γ), IFN- α 2, monocyte chemoattractant protein 1 (MCP-1), IL-8, IL-17A, and IL-18 (data not shown). These experiments demonstrated that S1 protein alone is sufficient to induce the upregulation of heparanase, which promotes the production of inflammatory cytokines. HPSE blockade with Ronaparstat dampens inflammatory cytokine release induced by SARS-CoV-2 S1 protein in macrophages.

SARS-CoV-2 spike protein-induced inflammatory cytokine release is partially mediated by HPSE. Heparanase is important for macrophage activation (25). To further investigate the proinflammatory role of HPSE in macrophages in the context of SARS-CoV-2, we knocked down the HPSE gene in the human macrophage cell line THP-1 using short hairpin RNA (shRNA) with a 60% average knockdown efficiency (Fig. 5A). THP-1 cell-derived macrophages were challenged with S1 protein (0.5 μ g/mL). The knockdown of HPSE in THP-1 macrophages prevented the induction of *IL6* or *IL1B* gene expression (Fig. 5B and C). At the protein level, using a flow cytometry-based multiplex inflammatory cytokine array, we found marked increases in multiple inflammatory cytokines (IL-6, TNF- α , MCP-1, and IL-1B) in the conditioned medium from the S1-stimulated THP-1 cells but at much lower levels in the stimulated HPSE knockdown lines (Fig. 5D to H). These data suggest that HPSE plays an important role in the induction of inflammation cytokines in macrophages upon S1 protein challenge.

Ronaparstat decreases SARS-CoV-2 spike protein-induced inflammatory cytokine release via NF- κ B signaling. NF- κ B signaling is a master regulator of inflammation, which regulates the transcription of several cytokines (26). To test whether the induction of the inflammatory cytokines by SARS-CoV-2 spike protein was dependent on NF- κ B signaling, human macrophages were pretreated with the NF- κ B inhibitor BAY-11-7082 (BAY) for 1 h, followed by S1 protein challenge. Treatment with BAY suppressed S1 protein-induced inflammatory cytokine gene expression (*IL6*, *TNF*, *IL1B*, and *CCL2*) in a dose-dependent manner (Fig. 6A to D). At steady state, cytosolic NF- κ B p65 is retained in an inactive form and is targeted by E3 ligases for degradation (27). In response to proinflammatory signals, p65 translocates from the cytoplasm to the nucleus, where it is stabilized and activates the transcription of inflammatory cytokine genes. In macrophages, p65 also induces its own transcription, further increasing the nuclear occupancy of p65 and, consequently, cytokine production (26). Immunostaining of p65 in primary macrophages stimulated with S1 protein showed an overall increase of p65, with a significant increase in nuclear occupancy, as measured by the nuclear mean fluorescence intensity (MFI). Cotreatment with Ronaparstat showed a dose-dependent reduction in nuclear p65 (Fig. 6E and F). The reduction of nuclear and cytoplasmic NF- κ B (p65) was also confirmed by Western blotting (Fig. 6G to I). Together, these data demonstrated that in macrophages

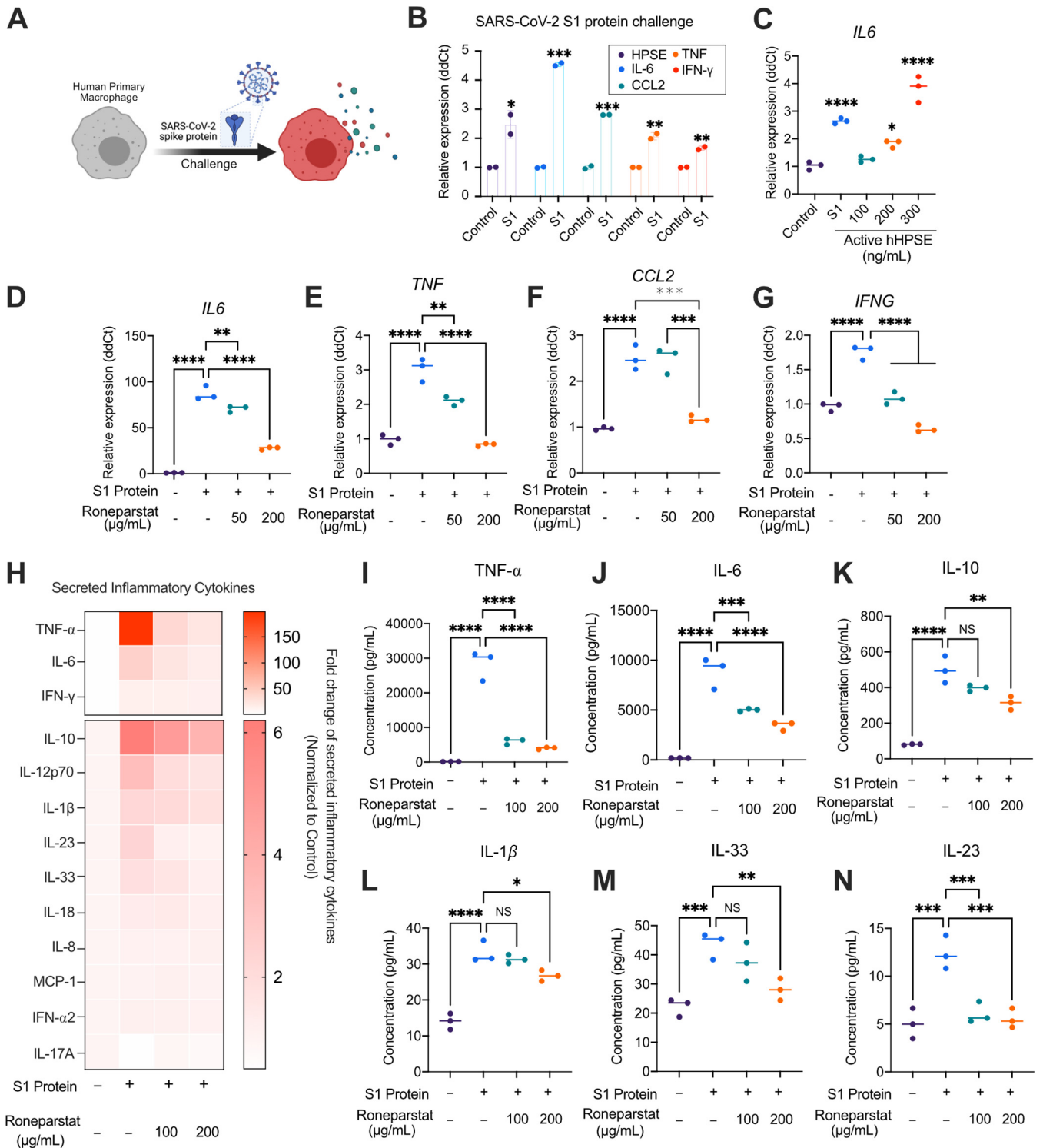


FIG 4 Inhibition of HPSE by Roneparstat decreases inflammatory cytokine release induced by the SARS-CoV-2 spike protein. (A) Experimental design of human primary monocyte-derived macrophages challenged with SARS-CoV-2 spike (S1) protein. (B) qPCR detection of the transcription of the *HPSE*, *IL6*, *TNF*, *CCL2*, and *IFNG* genes in macrophages challenged with S1 protein (0.5 μ g/mL) for 12 h. (C) qPCR detection of the transcription of *IL-6* in macrophages challenged with S1 protein (0.5 μ g/mL) or various doses (100, 200, and 300 ng/mL) of recombinant active heparanase (rHPSE) for 12 h. (D to G) qPCR detection of the transcription of the *IL6*, *TNF*, *CCL2*, and *IFNG* genes in macrophages cotreated with S1 protein (0.5 μ g/mL) and various doses of Roneparstat (50 and 200 μ g/mL) for 12 h. (H) Conditioned medium was collected from the macrophages cotreated with S1 protein (0.5 μ g/mL) and various doses of Roneparstat (100 and 200 μ g/mL) for 24 h. Inflammatory cytokines were quantified using a flow cytometry-based multiplex cytokine array. Fold changes of the secreted inflammatory cytokines were normalized to the values for the untreated control and are presented in a heat map. (I to N) Absolute concentrations of secreted TNF- α , IL-6, IL-10, IL-1 β , IL-33, and IL-23 were calculated based on standard curve fitting. Error bars represent the SEM. *, $P < 0.05$; **, $P < 0.01$; ***, $P < 0.001$ (2-tailed distribution, homoscedastic Student's t test for 2 groups or 1-way ANOVA for multiple comparisons).

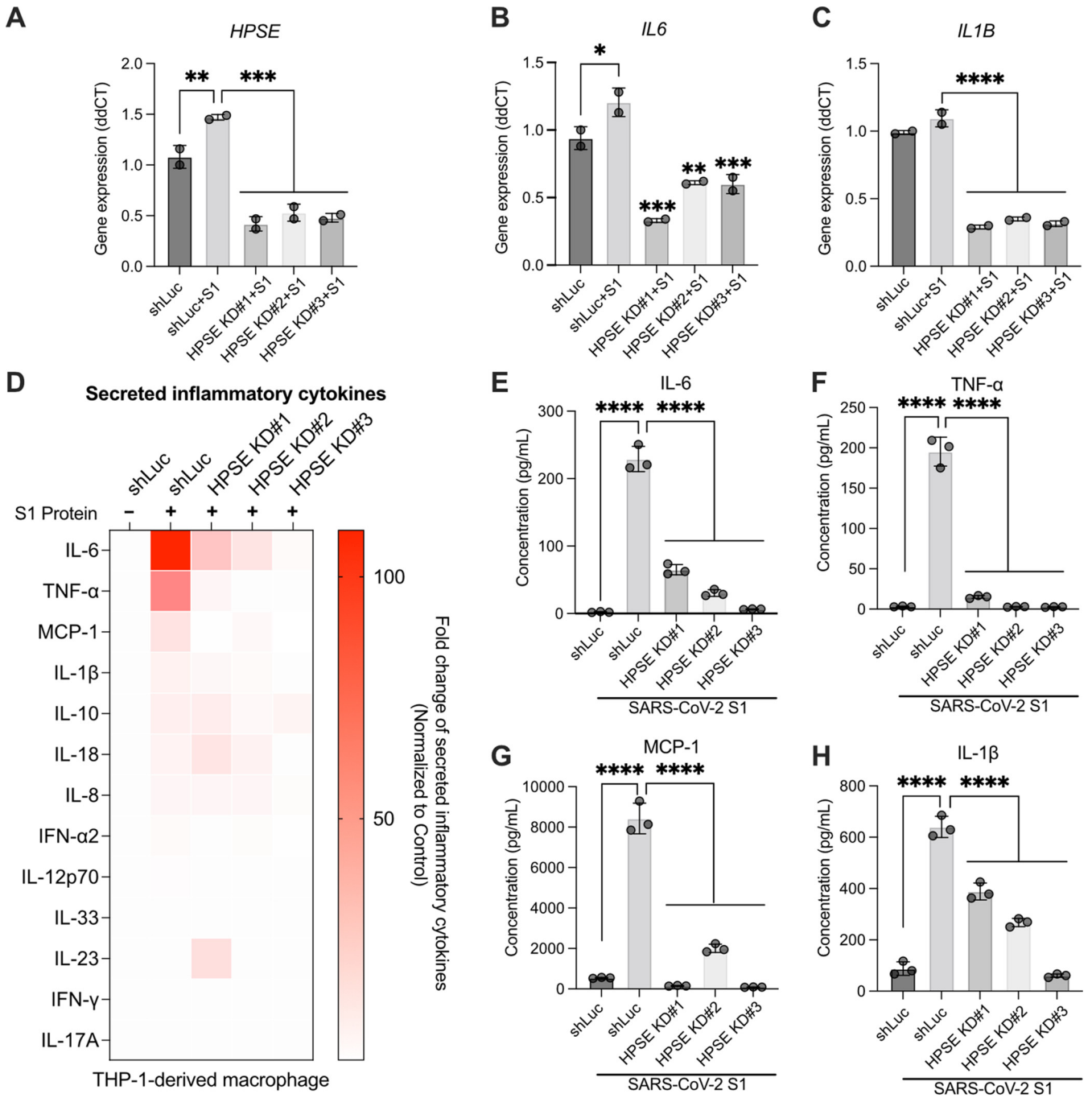


FIG 5 SARS-CoV-2 S1-induced inflammatory cytokine release depends on HPSE expression. Control (shLuc) or HPSE knockdown (KD) THP-1-derived macrophages were challenged with S1 protein (0.5 μg/mL) for 12 h. (A to C) Transcription levels of *HPSE* (A), *IL6* (B), and *IL1B* (C) were examined by qPCR. (D) Conditioned medium was collected from the THP-1 macrophages treated with S1 protein (0.5 μg/mL) for 24 h. Inflammatory cytokines were quantified using a flow cytometry-based multiplex cytokine array. Fold changes of the secreted inflammatory cytokines were normalized to the values for the untreated control and are presented in a heat map. (E to H) Absolute concentrations of secreted IL-6 (E), TNF-α (F), MCP-1 (G), and IL-1β (H) were calculated based on standard curve fitting. Error bars represent the SEM. *, $P < 0.05$; **, $P < 0.01$; ***, $P < 0.001$ (2-tailed distribution, homoscedastic Student's *t* test for 2 groups or 1-way ANOVA for multiple comparisons).

challenged with SARS-CoV-2 S1 protein, Ronaparstat treatment reduced NF-κB-dependent induction of inflammatory cytokines.

DISCUSSION

To date, COVID-19 has caused over 5 million deaths worldwide. However, while the development and deployment of vaccines are ongoing, effective therapy for COVID-19

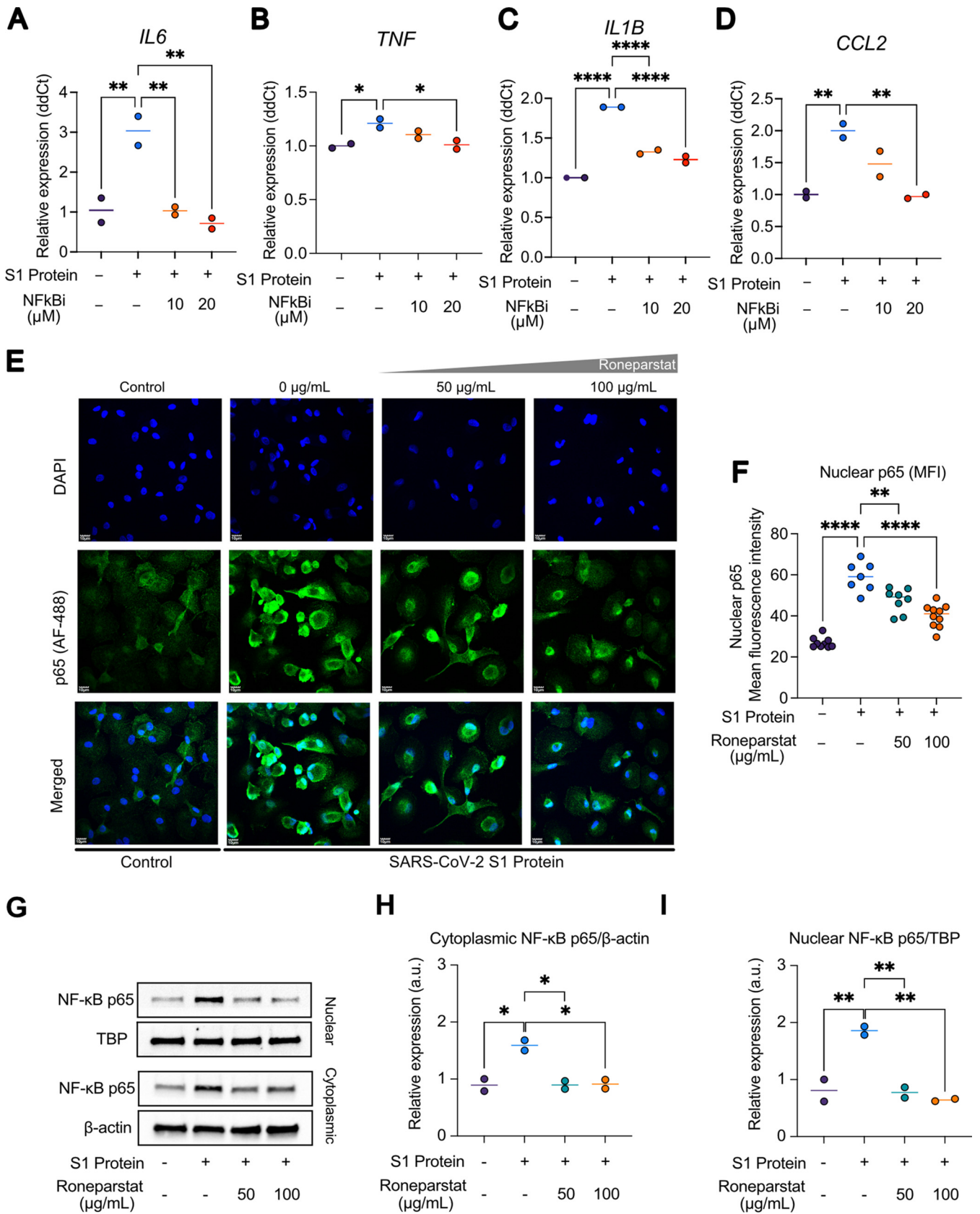


FIG 6 Roneparstat decreases SARS-CoV-2 spike protein-induced inflammatory cytokine release via NF-κB signaling. Human primary macrophages were pretreated with an NF-κB inhibitor (NFκBi) (BAY) for 1 h, followed by S1 protein (0.5 μg/mL) challenge for 12 h. (A to D) Transcription levels of *IL6* (A), *TNF* (Continued on next page)

is still urgently needed. In this study, we sought to evaluate the role of heparanase in COVID-19 disease pathology and to evaluate Ronaparstat, a chemically modified heparin that is a potent inhibitor of heparanase enzyme activity without anticoagulant activity, as a novel dual-targeting therapy for COVID-19. Many viruses, including SARS-CoV-2, are known to utilize heparan sulfate (HS) to attach to the host target cell. In line with these findings, we found that treatment with Ronaparstat significantly decreased infection by coronaviruses, including SARS-CoV-2 and SARS-CoV-1, as well as retroviruses, including HTLV-1 and HIV-1, *in vitro*. From scRNA-seq analyses of bronchoalveolar lavage fluid (BALF) samples from COVID-19 patients, we found that heparanase gene (*HPSE*) expression was significantly upregulated in CD68⁺ bronchial macrophages in COVID-19 patients with moderate and severe disease. To evaluate the role of heparanase in macrophages and inflammation in COVID-19, we stimulated human macrophages with SARS-CoV-2 S1 protein and found significant induction of heparanase and other key inflammatory cytokines. Importantly, we found that pharmacological blockade of heparanase with Ronaparstat suppressed inflammatory cytokine production in response to SARS-CoV-2 S1 protein challenge, through decreased NF- κ B signaling.

A recent structural analysis revealed that heparin, a structural analog of HS, can bind to the receptor binding domain (RBD) of the SARS-CoV-2 S1 protein, inducing a distinct conformational change (28). The interaction between heparin and the SARS-CoV-2 spike protein was also confirmed by competitive binding assays, showing that heparin can bind at high-picomolar affinity (29). Our data revealed that both heparin and Ronaparstat potently decreased infection by SARS-CoV-2 in Vero-E6 cells. Using the VSV-eGFP-SARS-CoV-2 chimeric virus, we observed similar potency of Ronaparstat or heparin in blocking infectivity, indicating that one of the main mechanisms leading to reduced infectivity could be through Ronaparstat competitive disruption of SARS-CoV-2 spike protein binding to cell surface HS. An extended analysis of Ronaparstat and infectivity using other RNA viruses, including VSV-eGFP-SARS-CoV-1 chimeric virus and pathogenic HIV-1 and HTLV-1, also showed the efficacy of Ronaparstat in reducing infection. Importantly, Ronaparstat failed to decrease the infectivity of VSVg-HIV-luc- Δ env, an HSPG-independent pseudotyped HIV-1. These data suggest that the reliance on HSPGs to enter the target cell may be a common phenomenon among these RNA viruses. Although beyond the scope of this study, we are designing experiments to determine if Ronaparstat interferes with the RBD of the SARS-CoV-2 spike protein, as has been observed with heparin.

Heparanase regulates the availability of HS on the cell surface or within the extracellular matrix. Upregulation of heparanase has been primarily studied for its role in cancer progression (12). In recent years, accumulating evidence suggests that HPSE is also involved in viral disease pathogenesis (30). In HSV-1-associated disease, the upregulation of HPSE after HSV-1 infection promoted virus shedding and the production of proinflammatory cytokines (31, 32). Another recent study reported by Agelidis et al. demonstrated that cells lacking HPSE expression are intrinsically resistant to HSV-1 infection. In the corneal infection model, HPSE knockout mice also had decreased virus titers and associated inflammation (33). The role of heparanase in viral pathogenesis is likely due to the multiple effects of this enzyme. Once new virus is produced, during its egress from the cell, it can be trapped on the cell surface by heparan sulfate-bearing cell surface proteoglycans, including syndecan-1. Heparanase stimulated by viral infection degrades cell surface heparan sulfate chains, thereby facilitating the release of the

FIG 6 Legend (Continued)

(B), *IL1B* (C), and *IFNG* (D) were assessed by qPCR. (E) Representative NF- κ B (p65) immunostaining of human primary macrophages cotreated with S1 protein (0.5 μ g/mL) and various doses of Ronaparstat (50 and 100 μ g/mL) for 24 h. (Top) DAPI; (middle) p65 (Alexa Fluor 488 [AF-488]); (bottom) merged. (F) Quantification of the mean fluorescence intensity (MFI) of the nuclear p65 signal. Seven to ten high-power fields were captured and quantified under each treatment condition. (G) Western blots of cytoplasmic and nuclear p65 in human primary macrophages treated with various doses of Ronaparstat (50 and 100 μ g/mL) and S1 protein (0.5 μ g/mL) for 30 min. Blots were reprobed with anti-TBP antibody as a loading control for nuclear fractions and β -actin for the cytoplasmic fractions. (H and I) Cytoplasmic and nuclear p65 levels were quantified by NF- κ B p65/ β -actin and p65/TBP ratios, respectively. a.u., arbitrary units. Error bars represent the SEM. *, $P < 0.05$; **, $P < 0.01$; ***, $P < 0.001$ (2-tailed distribution, homoscedastic Student's *t* test for 2 groups or 1-way ANOVA for multiple comparisons).

virus bound to those chains (30). An additional role for heparanase in viral egress lies in its ability to stimulate the shedding of heparan sulfate proteoglycans from the cell surface. It was previously demonstrated that the expression of heparanase by myeloma cells upregulates extracellular signal-regulated kinase (ERK) signaling, leading to the expression of the syndecan-1 sheddase matrix metalloproteinase 9 (MMP-9) (34). Similarly, during HSV-1 infection, heparanase induces the expression of MMP-3 and MMP-7, which leads to the shedding of cell surface syndecan-1 and the virus that is bound to the heparan sulfate chains (35).

The addition of purified recombinant heparanase resulted in macrophage activation and the upregulation of inflammatory cytokines, including IL-6 (36). Macrophages from heparanase knockout (Hpa-KO) mice also expressed lower levels of inflammatory cytokines (e.g., IL-6, TNF- α , and IL-1 β) (25), and the overexpression of *Hpse* exacerbated inflammatory cytokine production in an ulcerative colitis model (13). Buijssers et al. recently reported that elevated plasma levels of heparanase were detected in hospitalized patients with COVID-19 (16), but the source of heparanase has not been defined. In our studies, single-cell RNA-seq analysis of cells harvested from BALF enabled us to identify macrophages as the primary source of heparanase. In a recent report by Abdelmoaty et al. (37), it was shown that human macrophages were infected by live SARS-CoV-2. Although infection of macrophages by SARS-CoV-2 is restrictive without evidence of replication, mature virions showed long persistence (14 days after initial exposure). In addition, persistent SARS-CoV-2 components in macrophages induced the production of multiple proinflammatory cytokines such as IL-6, IL-1 β , and TNF- α , similar to what we have shown with the SARS-CoV-2 S1 protein, and HPSE knockdown in THP-1-derived macrophages resulted in a significant attenuation of inflammatory cytokines, highlighting the pivotal role of HPSE in the induction of inflammation. Together, these data demonstrated the multifaceted roles of heparanase in both infection and inflammation.

A subset of COVID-19 patients progress to a severe stage, characterized by dysregulated inflammatory cytokine release that causes tissue injury, acute respiratory distress syndrome (ARDS), and death. The hyperinflammatory state in patients with severe COVID-19 resembles cytokine release syndrome (CRS), which is seen in patients receiving chimeric antigen receptor (CAR) T-cell therapy (5). The overproduction of IL-6 by monocytes/macrophages has emerged as a key driver of CRS. Tocilizumab, a humanized monoclonal antibody against the IL-6 receptor, has been evaluated in large randomized clinical trials. While some trials (RECOVERY and REMAP-CAP trials) showed a survival benefit, others, including the COVACTA trial, showed a limited or no benefit in patient mortality (38, 39). These disparate results may be due to multiple factors, such as the timing of the treatment, the patient population, and the use of glucocorticoids. This may also indicate that targeting a single inflammatory cytokine may not be sufficient to suppress the overall inflammatory disease progression in COVID-19. In our cytokine screening of a panel of common proinflammatory cytokines, we found elevations of numerous inflammatory cytokines other than IL-6 after S1 protein challenge that were blocked by Ronaparstat, suggesting that targeting heparanase could be a viable therapeutic approach for inhibiting inflammatory cytokine release in COVID-19.

The NF- κ B signaling pathway is the main regulator of the production of inflammatory cytokines during the innate immune response. Wang et al. reported that the SARS-CoV-1 spike protein induced IL-6 and TNF- α production by activating NF- κ B (40). IL-6 is the main stimulator of STAT3, which allows the full activation of the NF- κ B signaling pathway (41). TNF- α also promotes the activation of noncanonical NF- κ B signaling. In the case of hyperinflammation, these interactions result in a vicious cycle of NF- κ B hyperactivation fueling the production and release of more inflammatory cytokines. In our study, Western blot assays as well as immunofluorescence staining of NF- κ B (p65) in macrophages showed increased p65 expression in both the cytoplasmic and nuclear compartments, suggesting that the spike protein is a strong activator of NF- κ B signaling. Treatment with Ronaparstat decreases both the cytoplasmic and nuclear

p65 levels, suggesting that heparanase inhibition could prevent the induction of the expression of p65. Studies are under way to evaluate NF- κ B signaling in infection and pathogenesis models *in vivo*.

Pulmonary activation of coagulation pathways is common in severe COVID-19, evidenced by the elevated levels of D-dimer and fibrin degradation product (FDP) (42). Patients with severe COVID-19 are at an increased risk of venous thromboembolism and microthrombosis. Disseminated intravascular coagulation (DIC) was reported in 71.4% of nonsurvivors versus 0.6% of survivors among patients diagnosed with COVID-19 (43). Anticoagulant therapy such as heparin was recommended for COVID-19 patients with hypercoagulable syndromes. From one retrospective study, treatment with low-molecular-weight heparin (LMWH) resulted in lower serum IL-6 levels in COVID-19 patients (44). No therapeutic benefit of heparin was observed in COVID-19 patients with critical disease (45). In COVID-19 patients with moderate disease, therapeutic doses of heparin increased the probability of survival and reduced the use of cardiovascular or respiratory organ support, compared with the usual-care thromboprophylaxis (46). The therapeutic dose of heparin, however, is associated with a 10 to 15% risk of significant bleeding. Factors increasing the risk of bleeding include older age, anemia, recent trauma or surgery, hypertension, and renal insufficiency. Many of these risk factors are common in patients with severe COVID-19. In contrast, Ronaparstat is a chemically modified heparin that caused little to no bleeding complications in a phase I clinical trial at all doses tested. In our infectivity assay, Ronaparstat showed activity comparable to that of unfractionated heparin in the SARS-CoV-2 infectivity assay. An open-label, multicenter phase I clinical trial (ClinicalTrials.gov identifier NCT01764880) was carried out to evaluate the safety and tolerability of Ronaparstat in patients with relapsed/refractory multiple myeloma. Ronaparstat was well tolerated in patients, with no dose-limiting toxicities (20). Future studies are under way to examine the tolerability and efficacy of Ronaparstat in SARS-CoV-2 animal models.

COVID-19 consists of two main pathogenic phases, progressing from the initial infection response phase dominated by SARS-CoV-2 entry and replication to the inflammatory response phase dominated by the host immune response. The current standard COVID-19 therapy includes antiviral therapy with remdesivir and anti-inflammatory drugs such as dexamethasone to decrease disease severity but showed less optimal results in reducing mortality. While cytokines produced during the infection may contribute to the worsening of the disease, they could also be important for the antimicrobial response. Therefore, blocking of inflammatory cytokine release alone at the early stage may impair the clearance of the virus and lead to delayed recovery from the disease. This might partially explain the poorer outcomes in mild COVID-19 patients receiving dexamethasone in the RECOVERY trial (ClinicalTrials.gov identifier NCT04381936) (47). The dual-targeting effect of Ronaparstat on both viral infection and macrophage-mediated inflammatory cytokine release (Fig. 7) and its safe profile in patients could be advantageous in this setting. Beyond the scope of COVID-19, HPSE may also play a role in other RNA virus-mediated diseases, such as respiratory syncytial virus (RSV) (48). Studies are under way to evaluate Ronaparstat in RSV-associated pathogenesis. In conclusion, our preclinical data suggest that heparanase is a target for SARS-CoV-2 pathogenesis and that Ronaparstat could serve as a novel dual-targeting agent for COVID-19.

MATERIALS AND METHODS

Cell lines and viral particles. Experiments involving HTLV-1 were performed under biosafety level 2 (BSL2) practices and procedures. Experiments involving HIV-1 and SARS-CoV-2 were performed at BSL3 facilities under BSL3 practices and procedures. The Jurkat-LTR-Luc reporter line, the HTLV-1-transformed lymphocytic cell line MT-2, and the human monocyte cell line THP-1 (ATCC) were maintained in RPMI 1640 supplemented with 10% fetal bovine serum (FBS). The Vero-E6 (ATCC) cell line and the human 293T cell line were maintained in Dulbecco's modified Eagle's medium (DMEM) supplemented with 10% FBS. The Jurkat-LTR-Luc reporter cell line is a human T-cell leukemia cell line engineered to express firefly luciferase under the control of the HTLV-1 long terminal repeat, as described previously (49). The TZM-Blue HIV-1 reporter cell line is a HeLa cell clone that expresses CD4, CXCR4, CCR5, and the firefly

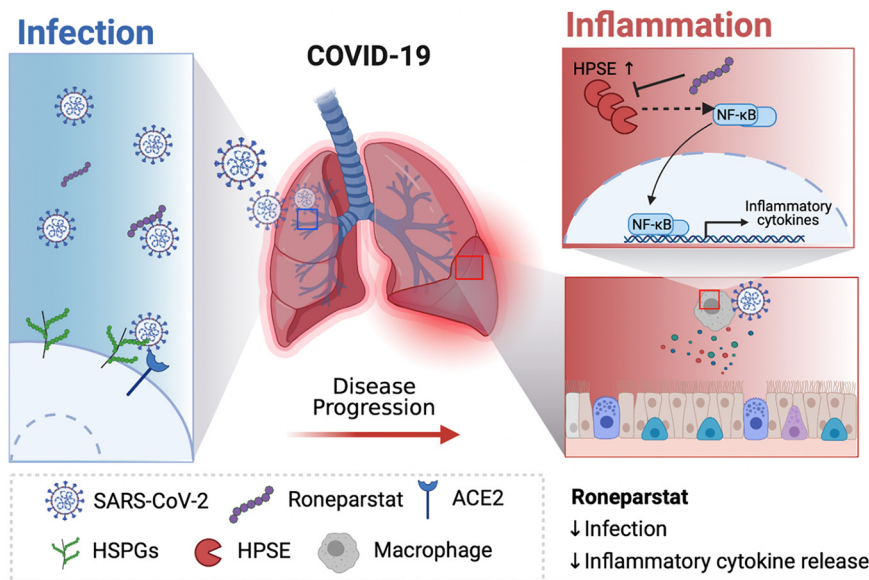


FIG 7 Schema of the potential dual-targeting actions of Roneparstat in COVID-19. The pathogenesis of COVID-19 consists of two pathogenic phases: (i) the early infection phase, characterized by SARS-CoV-2 viral entry, replication, and spread, and (ii) the later inflammation phase, characterized by aberrant proinflammatory cytokine release that leads to tissue damage, ARDS, or even death. During the initial infection phase, Roneparstat decreases viral infection by competing with HSPG-dependent viral entry. During the inflammation phase, HPSE blockade via Roneparstat attenuates SARS-CoV-2-mediated inflammatory cytokine release from macrophages, through disruption of NF- κ B signaling. Together, this study demonstrated the potential use of Roneparstat as a dual-targeting therapy for COVID-19 to decrease viral infection and dampen the proinflammatory immune response mediated by macrophages.

luciferase gene driven by the HIV-1 long terminal repeat (50). TZM-Blue and Lenti-X 293T cells (TaKaRa Bio) were maintained in DMEM supplemented with 10% FBS.

Human primary peripheral blood mononuclear cells (PBMCs) were acquired from deidentified donors at the Mississippi Valley Regional Blood Center. As determined by Washington University's HRPO (Human Research Protection Office) in 2009, these anonymous human blood cells are not considered human subject research. PBMCs were isolated using Ficoll-Paque Plus density gradient medium, at a density of 1.077 g/mL (catalog number 10771; Sigma), according to the manufacturer's instructions.

HIV-1 NLHX (CXCR4-tropic) or HIV-1 NLYU2 (CCR5-tropic) viral particles were made by transfecting 293T cells with HIV-1 NLHX or HIV-1 NLYU2 plasmids, as previously described (50).

The replication-competent vesicular stomatitis virus (VSV)-SARS-CoV-2 chimeric virus expressing enhanced green fluorescent protein (eGFP) (VSV-eGFP-SARS-CoV-2), in which VSV G was replaced with the SARS-CoV-2 S gene, was generously provided by Sean Whelan (51). A similar VSV-SARS-CoV-1 chimeric virus (VSV-eGFP-SARS-CoV-1) was also provided by Sean Whelan. Both VSV-eGFP-SARS-CoV-2 and VSV-eGFP-SARS-CoV-1 were grown in Vero-E6 cells.

Human macrophage differentiation. Human CD14⁺ monocytes were purified from human PBMCs of healthy donors using CD14⁺ beads (catalog number 130-050-201; Miltenyi Biotec), according to the manufacturer's instructions. Purified CD14⁺ monocytes were cultured in minimal essential medium alpha (α -MEM) supplemented with 10% FBS and 20 ng/mL human recombinant macrophage colony-stimulating factor (M-CSF) (catalog number 574804; BioLegend). Fresh media with M-CSF were changed every 3 days until the cells reached 70 to 80% confluence (days 12 to 14).

Human THP-1-derived macrophage differentiation. THP-1 macrophage differentiation was initiated by exposing the cells to 5 ng/mL phorbol-12-myristate-13-acetate (PMA) (catalog number 16561-29-8; Sigma-Aldrich) for 72 h. Subsequently, PMA was removed, and THP-1-derived macrophages were washed one time with phosphate-buffered saline (PBS) before S1 protein (0.5 μ g/mL; GenScript, Piscataway, NJ) challenge. RNA or medium supernatants were harvested 12 h or 24 h after S1 protein challenge, respectively.

Inhibitors/drugs. Roneparstat (previously named SST0001 or ¹⁰⁰ NA,RO-H) (18, 52) was kindly supplied by Leadiant Biosciences (Rome, Italy). A stock concentration of 50 mg/mL was prepared by solubilizing the drug in sterile water and stored at room temperature (up to 30 days). Heparin sodium salt from porcine intestinal mucosa (catalog number H3149; Sigma) was resuspended in PBS at a stock concentration of 25 mg/mL and stored at 4°C. The NF- κ B inhibitor BAY 11-7082 (catalog number B5556; Sigma) was solubilized in dimethyl sulfoxide (DMSO) at a stock concentration of 50 mM and stored at -20°C.

SARS-CoV-2 infectivity assay. SARS-CoV-2 (USA-WA1/2020) was obtained from BEI Resources. USA-WA1/2020 was isolated from an oropharyngeal swab from a COVID-19 patient in Washington. Viral

stocks were generated by infecting Vero-E6 cells at an MOI of 0.1 PFU. Both Roneparstat and heparin were subjected to 4-fold serial dilutions from 200 $\mu\text{g}/\text{mL}$ to 0.003 $\mu\text{g}/\text{mL}$, and each dilution was mixed with the same volume of SARS-CoV-2 (16,000 PFU/mL). Next, the mixture was transferred to confluent Vero-E6 cells in 48-well plates. The final concentrations of Roneparstat and heparin were ~ 100 to 0.0015 $\mu\text{g}/\text{mL}$, and the virus dose was 400 PFU/well. After a 1-h inoculation at 37°C in a CO₂ incubator, the mixture was removed from each well, and fresh DMEM supplemented with 2% FBS and a different dose of Roneparstat or heparin (~ 100 to 0.0015 $\mu\text{g}/\text{mL}$) was added (200 $\mu\text{L}/\text{well}$). At 24 h postinfection, the cell culture supernatant from each well was harvested for virus titration by a plaque assay on Vero-E6 cells. The half-maximal inhibitory concentration (IC₅₀) was calculated based on the viral titer from the plaque assay. The infected Vero-E6 cell monolayer was fixed with 300 μL of 4% neutral buffered formaldehyde at room temperature for 2 h, followed by immunostaining with anti-SARS-CoV-2 S or N antibody. Percent inhibition was calculated with the formula % inhibition = $100 - \text{titer}_{\text{treated}}/\text{titer}_{\text{untreated}} \times 100$. The curve fit and IC₅₀ were generated by Prism 8 [log(inhibitor) versus normalized response – variable slope].

VSV-SARS-CoV-2 infectivity assay. Each compound was diluted serially, 4-fold, from 50 $\mu\text{g}/\text{mL}$ to 0.0122 $\mu\text{g}/\text{mL}$ and incubated with VSV-eGFP-SARS-CoV-2 or VSV-eGFP-SARS-CoV-1 for 1 h at 37°C. The compound-virus mixtures were used to inoculate Vero-E6 cells (MOI = 0.1) in 96-well plates and incubated at 37°C for 1 h, after which the mixture was replaced with 200 μL of DMEM with 2% FBS containing 50 $\mu\text{g}/\text{mL}$ to 0.0122 $\mu\text{g}/\text{mL}$ of each compound. At 10 h postinoculation, cells were fixed in 2% formaldehyde for 30 min at room temperature and replaced with PBS. Viral infectivity was measured by automated enumeration of GFP-positive cells from captured images using a Cytation 5 automated fluorescence microscope (BioTek) and analyzed using Gen5 data analysis software (BioTek). Percent inhibition was calculated as $100 - \text{green cells with compound treatment}/\text{green cells with no compound treatment} \times 100$. The IC₅₀ of each peptide was determined by Prism 8 [log(inhibitor) versus normalized response – variable slope].

Plaque assays for SARS-CoV-2, VSV-eGFP-SARS-CoV-2, and VSV-eGFP-SARS-CoV-1. Confluent Vero-E6 cells in 12-well plates were infected with 10-fold serial dilutions of SARS-CoV-2, VSV-eGFP-SARS-CoV-2, or VSV-eGFP-SARS-CoV-1 in FBS-free DMEM. After absorption for 1 h at 37°C, the inoculum was removed, and 1 mL of a MEM overlay containing 0.25% low-melting-point agarose, 2% FBS, 0.12% sodium bicarbonate, 25 mM HEPES (pH 7.7), 2 mM L-glutamine, 100 $\mu\text{g}/\text{mL}$ of streptomycin, and 100 U/mL of penicillin was added. After incubation at 37°C for 2 days, wells were fixed with 10% neutral buffered formaldehyde for 2 h, the overlay was removed, the cells were stained with 0.05% (wt/vol) crystal violet, and the plaques were counted.

HTLV-1 infectivity assay. The infectivity of HTLV-1 was measured using the Jurkat-LTR-Luc reporter cell line as described previously (53). Briefly, the HTLV-1-producing cell line MT-2 was irradiated using an XCell50 cell irradiator (Kubtec Scientific) at 60 Gy and incubated with Jurkat-LTR-Luc reporters at a ratio of 20,000 MT-2 cells to 100,000 Jurkat-LTR-Luc cells (1:5 ratio). Various doses of Roneparstat were added at the same time of infection. At 24 or 48 h postinfection, cells were collected and lysed in luciferase cell culture lysis buffer (Promega). Luciferase activities were measured and presented as relative light units (RLU).

HIV-1 infectivity assay. TZM-Blue reporter cells were pretreated with the inhibitor in a 48-well plate for 24 h, and CXCR4- or CCR5-tropic HIV-1 strains were then added in the presence of various doses of Roneparstat or the vehicle. At 48 h postinfection, infected TZM-Blue cells were collected and lysed with 0.2% Triton X-100 in PBS. Luciferase activities were measured and presented as RLU. For VSVg-HIV-1-luc pseudotyped virus production, 293T cells were cotransfected with pHIV-1-luc/ Δenv and pVSVg, and virus was collected at 72 h posttransfection, as previously described (54, 55). U87/X4 or U87/R5 cells were seeded into a 48-well plate (2×10^4 cells per well) and infected with VSVg-HIV-1-luc in the presence or absence of various amounts of Roneparstat. Infected cells were lysed in a solution containing 100 μL PBS and 0.5% Triton X-100 at 48 h postinfection and examined for luciferase activity. Each infection/treatment was run in triplicates.

Lentivirus production and HPSE knockdown THP-1 cells. Lenti-X 293 cells were transfected with psPAX2, PMD2.G and plasmid of interest using Lipofectamine 3000 (Invitrogen), and the supernatant was harvested at 24 h posttransfection. For HPSE KD, short hairpin RNA (shRNA) constructs in pLKO.1 puro vectors were obtained from Sigma-Aldrich (luciferase shRNA [shLuc], 5'-CAGAATCGTCGTATGCAGTGA-3'; HPSE shRNA 1, 5'-GAGGAGAAGTTACGGTTGGAA-3'; HPSE shRNA 2, 5'-CCCAAGAAGGAATCAACCTTT-3'; HPSE shRNA 3, 5'-GCGAGGAGATTCTGTAACCTT-3'). THP-1 cells were infected with lentivirus overnight in the presence of 10 $\mu\text{g}/\text{mL}$ protamine sulfate. At 24 h postinfection, transduced cells were selected with 2 $\mu\text{g}/\text{mL}$ puromycin for 3 days. RNA or conditioned medium was harvested from macrophages challenged with SARS-CoV-2 S1 protein (0.5 $\mu\text{g}/\text{mL}$) for 12 h or 24 h, respectively.

Western blotting. Nuclear and cytoplasmic protein lysates were isolated from human macrophages using the NE-PER nuclear and cytoplasmic extraction kit (Thermo Scientific) supplemented with Halt protease inhibitor cocktail (Thermo Scientific) according to the manufacturer's protocol. Samples were separated on 4 to 20% Mini-Protein TGX precast protein gels (Bio-Rad) by SDS-PAGE and transferred onto Immobilon-P polyvinylidene difluoride (PVDF) membranes (EMD Millipore) overnight at 4°C. Membranes were incubated with NF- κB p65 (clone D14E12), TATA binding protein (TBP) (clone D5C9H), or β -actin (clone 13E5) primary antibodies (1:1,000; Cell Signaling), followed by horseradish peroxidase (HRP)-conjugated anti-rabbit secondary antibody (1:2,000; Cell Signaling). All antibodies were diluted in 1 \times Tris-buffered saline (TBS)-Tween (TBST) with 5% bovine serum albumin (BSA). Bands were developed by enhanced chemiluminescence and quantified using ImageJ software.

Human macrophage immunocytochemistry (ICC) staining. Human PBMCs were resuspended in α -MEM (supplemented with 10% FBS and human recombinant M-CSF at 20 ng/mL) and seeded onto coverslips (number 1.5 coverslip, 13-mm glass diameter; VWR) in 24-well plates. Cells were cultured for 2 days, and the nonadherent cells were then removed by sequential washes with Dulbecco's PBS (DPBS) (Gibco). Fresh media with M-CSF were changed every 2 to 3 days until the cells reached 70 to 80% confluence (days 5 to 7). Cells were challenged with SARS-CoV-2 S1 (0.5 μ g/mL) protein, with or without various doses of Roneparstat (50 μ g/mL and 100 μ g/mL), for 24 h. For immunostaining, each well was fixed with 4% paraformaldehyde (15 min at room temperature), followed by two washes with ice-cold TBS. Each coverslip was subsequently incubated with 0.2% Triton X-100 (Sigma) for 10 min, 10% goat serum (Cell Signaling) for 30 min, anti-human p65 primary antibody (1:700; Cell Signaling) overnight at 4°C, and Alexa Fluor 488-conjugated anti-rabbit antibody (1:400; Jackson ImmunoResearch) for 1 h, and nuclei were counterstained with 4',6-diamidino-2-phenylindole (DAPI) (catalog number 422801; BioLegend) for 5 min. Coverslips were mounted onto glass slides (VWR) with ProLong Gold antifade mountant (catalog number P10144; Life Technologies).

Confocal microscopy and nuclear p65 quantification. Slides were imaged with a confocal microscope (FluoView1200; Olympus) with a 40 \times water immersion lens objective. Seven to ten high-power fields were captured under each treatment condition. To quantify the nuclear p65 signal, captured images were analyzed using the Fiji imaging processing package with standard plug-ins (56). DAPI staining was used to determine nuclear segmentation and masking. Briefly, for each high-power field, binary image masks were created using a DAPI-positive single-channel image to define the nuclear region of interest (ROI). The image calculator was used to subtract the DAPI mask from the original p65 single-channel images to create images with p65 staining within the nuclear ROI. Image measurements of the p65 mean fluorescence intensities (MFIs) within the nuclear ROI were then determined by the mean gray value within the DAPI mask using an empirically derived threshold.

Quantitative real-time PCR (qRT-PCR) and primers. RNA was extracted from cells using an RNeasy kit (Qiagen), and cDNA was generated with qScript cDNA supermix (Quanta Bio). qPCR was performed with PerfeCTa SYBR green supermix reagent (Quanta Bio) on the Bio-Rad CFX96 machine, as previously described (57). Primers designed for qPCR are as follows: *HPSE* forward primer 5'-CTCTCTGCTCTGCCATCTTTAG-3' and reverse primer 5'-CCTCTGTTGCTATGAGGTTT-3', *IL6* forward primer 5'-CTCCATCCAGTTGCCTTCT-3' and reverse primer 5'-CTCCGACTTGTGAAGTGGTATAG-3', *TNF* forward primer 5'-CCAGGGACCTCTCTAATCA-3' and reverse primer 5'-TCAGCTTGAGGGTTTGCTAC-3', *CCL2* forward primer 5'-TCATAGCAGCCACCTTCATTC-3' and reverse primer 5'-CTCTGCACTGAGATCTTCTATTG-3', *IFNG* forward primer 5'-ATGTCCAACGCAAAGCAATAC-3' and reverse primer 5'-ACCTCGAACAGCATCTGAC-3', *HPRT* forward primer 5'-AGAATGTCTTGATTGTGGAAGA-3' and reverse primer 5'-ACCTTGACCATCTTTGGATTA-3', *IL1B* forward primer 5'-CAAAGCGGCCAGGATATAA-3' and reverse primer 5'-CTAGGGATTGAGTCCACATTCAG-3', and *GAPDH* forward primer 5'-AGGTGGTGTGAACGGATTTG-3' and reverse primer 5'-TGTAGACCATGTAGTTGAGGTC-3'.

Multiplex cytokine array. A bead-based human inflammatory cytokine array was performed using LEGENDplex human inflammation panel 1 (BioLegend). Human primary macrophages were cultured for 24 h in the presence of S protein, with or without various doses of Roneparstat (50 to 200 μ g/mL). Twenty-five microliters of the conditioned medium from various conditions was used to measure the secreted cytokines in each sample, according to the instructions from the manufacturer. The measurement was performed on a FACSCalibur flow cytometer (BD), and the data were analyzed using LEGENDplex software (BioLegend).

Single-cell RNA sequencing analysis. The R package Seurat was used for data scaling, dimensionality reduction, clustering, differential expression analysis, and visualization (58). First, the gene-barcode matrix was normalized using the LogNormalize method in the Seurat NormalizeData function with default parameters. Next, 2,000 variable genes were selected using the vst selection method in the Seurat FindVariableFeatures function. Subsequently, the filtered features were scaled using the Seurat ScaleData function with default parameters, where the two variables nCount_RNA and percent.mito were regressed out during the scaling process. The principal-component analysis (PCA) was performed using variable genes, and the top 50 principal components were used to perform UMAP, which maps cells into the two-dimensional space for visualization. Next, a k-nearest-neighbor-based clustering analysis was performed on the PCA-reduced data to identify cell clusters using the Seurat FindClusters function with the resolution set to 1.2. Based on the UMAP reduction results, the DimPlot and FeaturePlot functions in Seurat were respectively used to visualize the BALF cell clusters and highlight the HPSE gene expression levels across healthy control, moderate COVID-19, and severe COVID-19 samples (Fig. 3A).

The FindAllMarkers function in Seurat was used to perform the differential expression analysis (59). The Model-Based Analysis of Single Cell Transcriptomics (MAST) package was used in FindAllMarkers. For each of the major cell types, the averaged differential HPSE gene expression level was calculated for each COVID-19 sample relative to all of the healthy control cells (Fig. 3B). The HPSE gene in each cell type was considered significant for a COVID-19 sample if the *P* value was <0.05, adjusted by the false discovery rate using Bonferroni correction.

Macrophages were reintegrated with a new Seurat object. Macrophages from all samples were integrated using the top 50 dimensions of canonical correlation analysis and PCA, where the parameter k.filter was set to 115. Next, the average expression levels of the HPSE gene and the inflammatory cytokine genes *IL6*, *TNF*, *IL1B*, and *CCL2* were calculated using the Seurat AverageExpression function with default parameters. Similarly, average expression levels for each of the healthy control, moderate COVID-19, and severe COVID-19 samples were generated (Fig. 3C).

Statistical analysis. Experiments were analyzed using two-tailed Student's *t* test (2 groups), one-way analysis of variance (ANOVA) (>2 groups or repeated measures), or two-way ANOVA (two variables;

the *P* value refers to the interaction) using Prism 8 (GraphPad Software, Inc.). A nonparametric Spearman correlation coefficient test was adopted to determine statistically significant correlations between two groups. Results were considered to reach significance at a *P* value of ≤ 0.05 and are indicated with asterisks in the figures (*, $P \leq 0.05$; **, $P \leq 0.01$; ***, $P \leq 0.001$; ****, $P \leq 0.0001$). Data are presented as mean values; error bars represent the standard errors of the means (SEM).

ACKNOWLEDGMENTS

We thank Patrick Green and David Warren for their valuable expert suggestions and criticism. We thank Dennis Oakley, Crystal Idleburg, and Nitin Pokhrel for their technical assistance. We thank Sean Whelan for providing VSV-eGFP-SARS-CoV-2 for this study.

Conception and design, J.X. and K.N.W. Development of methodology, J.X., M.L., M.S., S.M., J.L., and K.N.W. Acquisition of data, J.X., M.L., M.S., X.C., K.K., S.M., J.L., and Y.Z. Analysis and interpretation of data, J.X., M.L., M.S., X.C., K.K., J.D., S.M., J.L., and K.N.W. Writing, review, and/or revision of the manuscript, all authors.

This research was supported by awards CA100730 (L.R., X.C., K.N.W., and D.J.V.), CA154737 (K.N.W.), CA097250 (K.N.W.), and CA216840 (K.N.W.). Additional funding support was provided by grants from the St. Louis Men's Group against Cancer, the Pat Burkhardt Breast Cancer Fund, and the Siteman Cancer Center. We also thank the Hope Center Alafi Neuroimaging Lab for use of the Nanozoomer (NIH shared instrumentation grant number S10RR027552). Confocal microscopy using the Olympus FluoView1200 instrument was performed in part through the use of the Washington University Center for Cellular Imaging (WUCCI) supported by the Washington University School of Medicine, the Children's Discovery Institute of Washington University and St. Louis Children's Hospital (CDI-CORE-2015-505 and CDI-CORE-2019-813), and the Foundation for Barnes-Jewish Hospital (3770 and 4642).

Roneparstat (SST0001) is a proprietary drug of Leadiant Biosciences S.p.A. A.N. is an employee of Leadiant Biosciences S.p.A. No potential conflicts of interest are disclosed by the other authors.

REFERENCES

- Alturki SO, Alturki SO, Connors J, Cusimano G, Kutzler MA, Izmirly AM, Haddad EK. 2020. The 2020 pandemic: current SARS-CoV-2 vaccine development. *Front Immunol* 11:1880. <https://doi.org/10.3389/fimmu.2020.01880>.
- Wiersinga WJ, Rhodes A, Cheng AC, Peacock SJ, Prescott HC. 2020. Pathophysiology, transmission, diagnosis, and treatment of coronavirus disease 2019 (COVID-19): a review. *JAMA* 324:782–793. <https://doi.org/10.1001/jama.2020.12839>.
- Siddiqi HK, Mehra MR. 2020. COVID-19 illness in native and immunosuppressed states: a clinical-therapeutic staging proposal. *J Heart Lung Transplant* 39:405–407. <https://doi.org/10.1016/j.healun.2020.03.012>.
- Wu Z, McGoogan JM. 2020. Characteristics of and important lessons from the coronavirus disease 2019 (COVID-19) outbreak in China: summary of a report of 72314 cases from the Chinese Center for Disease Control and Prevention. *JAMA* 323:1239–1242. <https://doi.org/10.1001/jama.2020.2648>.
- Fajgenbaum DC, June CH. 2020. Cytokine storm. *N Engl J Med* 383:2255–2273. <https://doi.org/10.1056/NEJMra2026131>.
- Shang J, Wan Y, Luo C, Ye G, Geng Q, Auerbach A, Li F. 2020. Cell entry mechanisms of SARS-CoV-2. *Proc Natl Acad Sci U S A* 117:11727–11734. <https://doi.org/10.1073/pnas.2003138117>.
- Dai L, Gao GF. 2021. Viral targets for vaccines against COVID-19. *Nat Rev Immunol* 21:73–82. <https://doi.org/10.1038/s41577-020-00480-0>.
- Clausen TM, Sandoval DR, Spliid CB, Pihl J, Perrett HR, Painter CD, Narayanan A, Majowicz SA, Kwong EM, McVicar RN, Thacker BE, Glass CA, Yang Z, Torres JL, Golden GJ, Bartels PL, Porell RN, Garretson AF, Laubach L, Feldman J, Yin X, Pu Y, Hauser BM, Caradonna TM, Kellman BP, Martino C, Gordts PLSM, Chanda SK, Schmidt AG, Godula K, Leibel SL, Jose J, Corbett KD, Ward AB, Carlin AF, Esko JD. 2020. SARS-CoV-2 infection depends on cellular heparan sulfate and ACE2. *Cell* 183:1043–1057.e15. <https://doi.org/10.1016/j.cell.2020.09.033>.
- Cagno V, Tseligka ED, Jones ST, Tapparel C. 2019. Heparan sulfate proteoglycans and viral attachment: true receptors or adaptation bias? *Viruses* 11:596. <https://doi.org/10.3390/v11070596>.
- Rivara S, Milazzo FM, Giannini G. 2016. Heparanase: a rainbow pharmacological target associated to multiple pathologies including rare diseases. *Future Med Chem* 8:647–680. <https://doi.org/10.4155/fmc-2016-0012>.
- Vlodavsky I, Singh P, Boyango I, Gutter-Kapon L, Elkin M, Sanderson RD, Ilan N. 2016. Heparanase: from basic research to therapeutic applications in cancer and inflammation. *Drug Resist Updat* 29:54–75. <https://doi.org/10.1016/j.drug.2016.10.001>.
- Sanderson RD, Elkin M, Rapraeger AC, Ilan N, Vlodavsky I. 2017. Heparanase regulation of cancer, autophagy and inflammation: new mechanisms and targets for therapy. *FEBS J* 284:42–55. <https://doi.org/10.1111/febs.13932>.
- Lerner I, Hermano E, Zcharia E, Rodkin D, Bulvik R, Doviner V, Rubinstein AM, Ishai-Michaeli R, Atzmon R, Sherman Y, Meirovitz A, Peretz T, Vlodavsky I, Elkin M. 2011. Heparanase powers a chronic inflammatory circuit that promotes colitis-associated tumorigenesis in mice. *J Clin Invest* 121:1709–1721. <https://doi.org/10.1172/JCI43792>.
- Schmidt EP, Yang Y, Janssen WJ, Gandjeva A, Perez MJ, Barthel L, Zemans RL, Bowman JC, Koyanagi DE, Yunt ZX, Smith LP, Cheng SS, Overdier KH, Thompson KR, Geraci MW, Douglas IS, Pearse DB, Tuder RM. 2012. The pulmonary endothelial glycocalyx regulates neutrophil adhesion and lung injury during experimental sepsis. *Nat Med* 18:1217–1223. <https://doi.org/10.1038/nm.2843>.
- Koganti R, Suryawanshi R, Shukla D. 2020. Heparanase, cell signaling, and viral infections. *Cell Mol Life Sci* 77:5059–5077. <https://doi.org/10.1007/s00018-020-03559-y>.
- Buijssers B, Yanginlar C, de Nooijer A, Grondman I, Maciej-Hulme ML, Jonkman I, Janssen NAF, Rother N, de Graaf M, Pickkers P, Kox M, Joosten LAB, Nijenhuis T, Netea MG, Hilbrands L, van de Veerdonk FL, Duivenvoorden R, de Mast Q, van der Vlag J. 2020. Increased plasma heparanase activity in COVID-19 patients. *Front Immunol* 11:575047. <https://doi.org/10.3389/fimmu.2020.575047>.
- Pala D, Rivara S, Mor M, Milazzo FM, Roscilli G, Pavoni E, Giannini G. 2016. Kinetic analysis and molecular modeling of the inhibition mechanism of

- roneparstat (SST0001) on human heparanase. *Glycobiology* 26:640–654. <https://doi.org/10.1093/glycob/cww003>.
18. Naggi A, Casu B, Perez M, Torri G, Cassinelli G, Penco S, Pisano C, Giannini G, Ishai-Michaeli R, Vlodavsky I. 2005. Modulation of the heparanase-inhibiting activity of heparin through selective desulfation, graded N-acetylation, and glycol splitting. *J Biol Chem* 280:12103–12113. <https://doi.org/10.1074/jbc.M414217200>.
 19. Nosedà A, Barbieri P. 2020. Roneparstat: development, preclinical and clinical studies. *Adv Exp Med Biol* 1221:523–538. https://doi.org/10.1007/978-3-030-34521-1_21.
 20. Galli M, Chatterjee M, Grasso M, Specchia G, Magen H, Einsele H, Celeghini I, Barbieri P, Paoletti D, Pace S, Sanderson RD, Rambaldi A, Nagler A. 2018. Phase I study of the heparanase inhibitor roneparstat: an innovative approach for multiple myeloma therapy. *Haematologica* 103:e469–e472. <https://doi.org/10.3324/haematol.2017.182865>.
 21. Jones KS, Petrow-Sadowski C, Bertolette DC, Huang Y, Ruscetti FW. 2005. Heparan sulfate proteoglycans mediate attachment and entry of human T-cell leukemia virus type 1 virions into CD4⁺ T cells. *J Virol* 79:12692–12702. <https://doi.org/10.1128/JVI.79.20.12692-12702.2005>.
 22. Nasimuzzaman M, Persons DA. 2012. Cell membrane-associated heparan sulfate is a receptor for prototype foamy virus in human, monkey, and rodent cells. *Mol Ther* 20:1158–1166. <https://doi.org/10.1038/mt.2012.41>.
 23. Liao M, Liu Y, Yuan J, Wen Y, Xu G, Zhao J, Cheng L, Li J, Wang X, Wang F, Liu L, Amit I, Zhang S, Zhang Z. 2020. Single-cell landscape of bronchoalveolar immune cells in patients with COVID-19. *Nat Med* 26:842–844. <https://doi.org/10.1038/s41591-020-0901-9>.
 24. Herold T, Jurinovic V, Arnreich C, Lipworth BJ, Hellmuth JC, von Bergwelt-Baildon M, Klein M, Weinberger T. 2020. Elevated levels of IL-6 and CRP predict the need for mechanical ventilation in COVID-19. *J Allergy Clin Immunol* 146:128–136.e4. <https://doi.org/10.1016/j.jaci.2020.05.008>.
 25. Gutter-Kapon L, Alishekevitz D, Shaked Y, Li JP, Aronheim A, Ilan N, Vlodavsky I. 2016. Heparanase is required for activation and function of macrophages. *Proc Natl Acad Sci U S A* 113:E7808–E7817. <https://doi.org/10.1073/pnas.1611380113>.
 26. Dorrington MG, Fraser IDC. 2019. NF-kappaB signaling in macrophages: dynamics, crosstalk, and signal integration. *Front Immunol* 10:705. <https://doi.org/10.3389/fimmu.2019.00705>.
 27. Mitxitorena I, Somma D, Mitchell JP, Lepisto M, Tyrchan C, Smith EL, Kiely PA, Walden H, Keeshan K, Carmody RJ. 2020. The deubiquitinase USP7 uses a distinct ubiquitin-like domain to deubiquitinate NF-kB subunits. *J Biol Chem* 295:11754–11763. <https://doi.org/10.1074/jbc.RA120.014113>.
 28. Mycroft-West CJ, Su D, Pagani I, Rudd TR, Elli S, Gandhi NS, Guimond SE, Miller GJ, Meneghetti MCZ, Nader HB, Li Y, Nunes QM, Procter P, Mancini N, Clementi M, Bisio A, Forsyth NR, Ferro V, Turnbull JE, Guerrini M, Fernig DG, Vicenzi E, Yates EA, Lima MA, Skidmore MA. 2020. Heparin inhibits cellular invasion by SARS-CoV-2: structural dependence of the interaction of the spike S1 receptor-binding domain with heparin. *Thromb Haemost* 120:1700–1715. <https://doi.org/10.1055/s-0040-1721319>.
 29. Kim SY, Jin W, Sood A, Montgomery DW, Grant OC, Fuster MM, Fu L, Dordick JS, Woods RJ, Zhang F, Linhardt RJ. 2020. Characterization of heparin and severe acute respiratory syndrome-related coronavirus 2 (SARS-CoV-2) spike glycoprotein binding interactions. *Antiviral Res* 181:104873. <https://doi.org/10.1016/j.antiviral.2020.104873>.
 30. Agelidis A, Shukla D. 2020. Heparanase, heparan sulfate and viral infection. *Adv Exp Med Biol* 1221:759–770. https://doi.org/10.1007/978-3-030-34521-1_32.
 31. Hadigal SR, Agelidis AM, Karasneh GA, Antoine TE, Yakoub AM, Ramani VC, Djalilian AR, Sanderson RD, Shukla D. 2015. Heparanase is a host enzyme required for herpes simplex virus-1 release from cells. *Nat Commun* 6:6985. <https://doi.org/10.1038/ncomms7985>.
 32. Agelidis AM, Hadigal SR, Jaishankar D, Shukla D. 2017. Viral activation of heparanase drives pathogenesis of herpes simplex virus-1. *Cell Rep* 20:439–450. <https://doi.org/10.1016/j.celrep.2017.06.041>.
 33. Agelidis A, Turturice BA, Suryawanshi RK, Yadavalli T, Jaishankar D, Ames J, Hopkins J, Koujah L, Patil CD, Hadigal SR, Kyzar EJ, Campeau A, Wozniak JM, Gonzalez DJ, Vlodavsky I, Li J-P, Perkins DL, Finn PW, Shukla D. 2021. Disruption of innate defense responses by endoglycosidase HPSE promotes cell survival. *JCI Insight* 6:e144255. <https://doi.org/10.1172/jci.insight.144255>.
 34. Purushothaman A, Chen L, Yang Y, Sanderson RD. 2008. Heparanase stimulation of protease expression implicates it as a master regulator of the aggressive tumor phenotype in myeloma. *J Biol Chem* 283:32628–32636. <https://doi.org/10.1074/jbc.M806266200>.
 35. Hadigal S, Koganti R, Yadavalli T, Agelidis A, Suryawanshi R, Shukla D. 2020. Heparanase-regulated syndecan-1 shedding facilitates herpes simplex virus 1 egress. *J Virol* 94:e01672–19. <https://doi.org/10.1128/JVI.01672-19>.
 36. Masola V, Zaza G, Bellin G, Dall’Omo L, Granata S, Vischini G, Secchi MF, Lupo A, Gambaro G, Onisto M. 2018. Heparanase regulates the M1 polarization of renal macrophages and their crosstalk with renal epithelial tubular cells after ischemia/reperfusion injury. *FASEB J* 32:742–756. <https://doi.org/10.1096/fj.201700597R>.
 37. Abdelmoaty MM, Yeapuri P, Machhi J, Olson KE, Shahjin F, Kumar V, Zhou Y, Liang J, Pandey K, Acharya A, Byrareddy SN, Mosley RL, Gendelman HE. 2021. Defining the innate immune responses for SARS-CoV-2-human macrophage interactions. *Front Immunol* 12:741502. <https://doi.org/10.3389/fimmu.2021.741502>.
 38. Rosas IO, Brau N, Waters M, Go RC, Hunter BD, Bhagani S, Skiest D, Aziz MS, Cooper N, Douglas IS, Savic S, Youngstein T, Del Sorbo L, Cubillo Gracian A, De La Zerdá DJ, Ustianowski A, Bao M, Dimonaco S, Graham E, Matharu B, Spotswood H, Tsai L, Malhotra A. 2021. Tocilizumab in hospitalized patients with severe Covid-19 pneumonia. *N Engl J Med* 384:1503–1516. <https://doi.org/10.1056/NEJMoa2028700>.
 39. REMAP-CAP Investigators, Gordon AC, Mouncey PR, Al-Beidh F, Rowan KM, Nichol AD, Arabi YM, Annane D, Beane A, van Bentum-Puijk W, Berry LR, Bhimani Z, Bonten MJM, Bradbury CA, Brunkhorst FM, Buzgau A, Cheng AC, Detry MA, Duffy EJ, Estcourt LJ, Fitzgerald M, Goossens H, Haniffa R, Higgins AM, Hills TE, Horvat C, Lamontagne F, Lawler PR, Leavis HL, Linsrum KM, Litton E, Lorenzi E, Marshall JC, Mayr FB, McAuley DF, McGlothlin A, McGuinness SP, McVerry BJ, Montgomery SK, Morpeth SC, Murthy S, Orr K, Parke RL, Parker JC, Patanwala AE, Pettit V, Rademaker E, Santos MS, Saunders CT, Seymour CW, et al. 2021. Interleukin-6 receptor antagonists in critically ill patients with Covid-19. *N Engl J Med* 384:1491–1502. <https://doi.org/10.1056/NEJMoa2100433>.
 40. Wang W, Ye L, Ye L, Li B, Gao B, Zeng Y, Kong L, Fang X, Zheng H, Wu Z, She Y. 2007. Up-regulation of IL-6 and TNF-alpha induced by SARS-coronavirus spike protein in murine macrophages via NF-kappaB pathway. *Virus Res* 128:1–8. <https://doi.org/10.1016/j.virusres.2007.02.007>.
 41. Murakami M, Kamimura D, Hirano T. 2019. Pleiotropy and specificity: insights from the interleukin 6 family of cytokines. *Immunity* 50:812–831. <https://doi.org/10.1016/j.immuni.2019.03.027>.
 42. Jose RJ, Manuel A. 2020. COVID-19 cytokine storm: the interplay between inflammation and coagulation. *Lancet Respir Med* 8:e46–e47. [https://doi.org/10.1016/S2213-2600\(20\)30216-2](https://doi.org/10.1016/S2213-2600(20)30216-2).
 43. Tang N, Li D, Wang X, Sun Z. 2020. Abnormal coagulation parameters are associated with poor prognosis in patients with novel coronavirus pneumonia. *J Thromb Haemost* 18:844–847. <https://doi.org/10.1111/jth.14768>.
 44. Shi C, Wang C, Wang H, Yang C, Cai F, Zeng F, Cheng F, Liu Y, Zhou T, Deng B, Vlodavsky I, Li J-P, Zhang Y. 2020. The potential of low molecular weight heparin to mitigate cytokine storm in severe COVID-19 patients: a retrospective cohort study. *Clin Transl Sci* 13:1087–1095. <https://doi.org/10.1111/cts.12880>.
 45. REMAP-CAP Investigators, ACTIV-4a Investigators, ATTACC Investigators, Goligher EC, Bradbury CA, McVerry BJ, Lawler PR, Berger JS, Gong MN, Carrier M, Reynolds HR, Kumar A, Turgeon AF, Kornblith LZ, Kahn SR, Marshall JC, Kim KS, Houston BL, Derde LPG, Cushman M, Tritschler T, Angus DC, Godoy LC, McQuilten Z, Kirwan B-A, Farkouh ME, Brooks MM, Lewis RJ, Berry LR, Lorenzi E, Gordon AC, Ahuja T, Al-Beidh F, Annane D, Arabi YM, Aryal D, Baumann Kreuziger L, Beane A, Bhimani Z, Bihari S, Billett HH, Bond L, Bonten M, Brunkhorst F, Buxton M, Buzgau A, Castellucci LA, Chekuri S, Chen J-T, Cheng AC, et al. 2021. Therapeutic anticoagulation with heparin in critically ill patients with Covid-19. *N Engl J Med* 385:777–789. <https://doi.org/10.1056/NEJMoa2103417>.
 46. ATTACC Investigators, ACTIV-4a Investigators, REMAP-CAP Investigators, Lawler PR, Goligher EC, Berger JS, Neal MD, McVerry BJ, Nicolau JC, Gong MN, Carrier M, Rosenson RS, Reynolds HR, Turgeon AF, Escobedo J, Huang DT, Bradbury CA, Houston BL, Kornblith LZ, Kumar A, Kahn SR, Cushman M, McQuilten Z, Slutsky AS, Kim KS, Gordon AC, Kirwan B-A, Brooks MM, Higgins AM, Lewis RJ, Lorenzi E, Berry SM, Berry LR, Aday AW, Al-Beidh F, Annane D, Arabi YM, Aryal D, Baumann Kreuziger L, Beane A, Bhimani Z, Bihari S, Billett HH, Bond L, Bonten M, Brunkhorst F, Buxton M, Buzgau A, Castellucci LA, Chekuri S, et al. 2021. Therapeutic anticoagulation with heparin in noncritically ill patients with Covid-19. *N Engl J Med* 385:790–802. <https://doi.org/10.1056/NEJMoa2105911>.
 47. RECOVERY Collaborative Group, Horby P, Lim WS, Emberson JR, Mafham M, Bell JL, Linsell L, Staplin N, Brightling C, Ustianowski A, Elmahi E, Prudon B, Green C, Felton T, Chadwick D, Rege K, Fegan C, Chappell LC, Faust SN, Jaki T, Jeffery K, Montgomery A, Rowan K, Juszczak E, Baillie JK, Haynes R, Landray

- MJ. 2021. Dexamethasone in hospitalized patients with Covid-19. *N Engl J Med* 384:693–704. <https://doi.org/10.1056/NEJMoa2021436>.
48. Tao Y-H, Wang Z, Zhou Y-R. 2014. Expression of heparanase in kidney of rats with respiratory syncytial virus nephropathy and its relationship with proteinuria [sic]. *Sichuan Da Xue Xue Bao Yi Xue Ban* 45:212–215, 224. (In Chinese).
49. Pais-Correia AM, Sachse M, Guadagnini S, Robbiati V, Lasserre R, Gessain A, Gout O, Alcover A, Thoulouze MI. 2010. Biofilm-like extracellular viral assemblies mediate HTLV-1 cell-to-cell transmission at virological synapses. *Nat Med* 16:83–89. <https://doi.org/10.1038/nm.2065>.
50. Harmon B, Campbell N, Ratner L. 2010. Role of Abl kinase and the Wave2 signaling complex in HIV-1 entry at a post-hemifusion step. *PLoS Pathog* 6:e1000956. <https://doi.org/10.1371/journal.ppat.1000956>.
51. Case JB, Rothlauf PW, Chen RE, Liu Z, Zhao H, Kim AS, Bloyet L-M, Zeng Q, Tahan S, Droit L, Ilagan MXG, Tartell MA, Amarasinghe G, Henderson JP, Miersch S, Ustav M, Sidhu S, Virgin HW, Wang D, Ding S, Corti D, Theel ES, Fremont DH, Diamond MS, Whelan SPJ. 2020. Neutralizing antibody and soluble ACE2 inhibition of a replication-competent VSV-SARS-CoV-2 and a clinical isolate of SARS-CoV-2. *Cell Host Microbe* 28:475–485.e5. <https://doi.org/10.1016/j.chom.2020.06.021>.
52. Ritchie JP, Ramani VC, Ren Y, Naggi A, Torri G, Casu B, Penco S, Pisano C, Carminati P, Tortoreto M, Zunino F, Vlodavsky I, Sanderson RD, Yang Y. 2011. SST0001, a chemically modified heparin, inhibits myeloma growth and angiogenesis via disruption of the heparanase/syndecan-1 axis. *Clin Cancer Res* 17:1382–1393. <https://doi.org/10.1158/1078-0432.CCR-10-2476>.
53. Alais S, Dutartre H, Mahieux R. 2017. Quantitative analysis of human T-lymphotropic virus type 1 (HTLV-1) infection using co-culture with Jurkat LTR-luciferase or Jurkat LTR-GFP reporter cells. *Methods Mol Biol* 1582: 47–55. https://doi.org/10.1007/978-1-4939-6872-5_4.
54. Landau NR, Page KA, Littman DR. 1991. Pseudotyping with human T-cell leukemia virus type I broadens the human immunodeficiency virus host range. *J Virol* 65:162–169. <https://doi.org/10.1128/JVI.65.1.162-169.1991>.
55. Harmon B, Ratner L. 2008. Induction of the Galpha(q) signaling cascade by the human immunodeficiency virus envelope is required for virus entry. *J Virol* 82:9191–9205. <https://doi.org/10.1128/JVI.00424-08>.
56. Schindelin J, Arganda-Carreras I, Frise E, Kaynig V, Longair M, Pietzsch T, Preibisch S, Rueden C, Saalfeld S, Schmid B, Tinevez JY, White DJ, Hartenstein V, Eliceiri K, Tomancak P, Cardona A. 2012. Fiji: an open-source platform for biological-image analysis. *Nat Methods* 9:676–682. <https://doi.org/10.1038/nmeth.2019>.
57. Xiang J, Rauch DA, Huey DD, Panfil AR, Cheng X, Esser AK, Su X, Harding JC, Xu Y, Fox GC, Fontana F, Kobayashi T, Su J, Sundaramoorthi H, Wong WH, Jia Y, Rosol TJ, Veis DJ, Green PL, Niewiesk S, Ratner L, Weilbaecher KN. 2019. HTLV-1 viral oncogene HBZ drives bone destruction in adult T cell leukemia. *JCI Insight* 4:e128713. <https://doi.org/10.1172/jci.insight.128713>.
58. Butler A, Hoffman P, Smibert P, Papalexi E, Satija R. 2018. Integrating single-cell transcriptomic data across different conditions, technologies, and species. *Nat Biotechnol* 36:411–420. <https://doi.org/10.1038/nbt.4096>.
59. Finak G, McDavid A, Yajima M, Deng J, Gersuk V, Shalek AK, Slichter CK, Miller HW, McElrath MJ, Prlic M, Linsley PS, Gottardo R. 2015. MAST: a flexible statistical framework for assessing transcriptional changes and characterizing heterogeneity in single-cell RNA sequencing data. *Genome Biol* 16:278. <https://doi.org/10.1186/s13059-015-0844-5>.